The Application of Acceleration Frequency Domain Factors in the Analysis of Headform Impacts

Evan Walsh

School of Kinesiology

Lakehead University

14 October 2008

TABLE OF CONTENTS

TABLE OF FIGURES

LIST OF EQUATIONS

LIST OF TABLES

INTRODUCTION

In the field of head injury prevention, many factors have been investigated with respect to understanding determinants of injury (Gurdjian & Gurdjian, 1978). Both occurrence and severity of head trauma as a result of mechanical impacts from a large variety of direct and indirect sources have been studied in an effort to quantify the likelihood of head injury (Got, Patel, Fayon, Tarrière, & Walfisch, 1993). Although people have been wearing helmets for millennia to prevent head injuries, it was not until the twentieth century that a working definition of head injury prediction was developed accounting for biomechanical factors (Gurdjian, 1975).

In the 1930s, Scott experimented on laboratory animals and established correlations between increases in intracranial pressure, as a result of direct head impacts resulting in concussive symptoms (Gurdjian, 1975; Ward, Chan, & Nahum, 1993). This work was followed by several researchers in the 1940s, namely Denny-Brown, Russel, Gurdjian, Webster, Walker, Lissner, as well as many others, who began quantifying similar biomechanical parameters recorded in laboratory based head impact studies. Specifically, impact and resulting head velocity, impact energy, and duration of impact were each investigated in the early head injury determination experiments (Gurdjian, 1975).

In 1966, Gadd, an automotive engineer at General Motors, derived a severity index equation using the total linear acceleration and deceleration experienced by the head as a result of direct and indirect blows. Any acceleration measures causing a score above a threshold value established by Gadd based on laboratory data were deemed to be deleterious (Gadd, 1993). Although the concept established by Gadd was

groundbreaking for its ability to predict potential head trauma danger using a standardized approach, the inclusion of both the initial head acceleration as well as rebound acceleration proved to be inaccurate in predicting injury for many cases (Gurdjian, 1975).

In addition to the research by Gadd, studies were being conducted at Wayne State University in Detroit, Michigan, by a group of researchers that included Patrick, Mertz, Kroell, Gurdjian, and Hodgson (Gurdjian, 1975; Versace, 1993). A series of experiments established a set of threshold data, as shown in Table 1, using post mortem human and live animal subjects. Impactors weighing approximately 0.86 kg were used to cause head impacts which resulted in velocities ranging between 13.1 to $14.3\frac{m}{s}$. The results of these initial impacts were used to predict a critical linear acceleration that was considered to be intolerable by the adult human as a result of direct head impact (Gurdjian, 1975).

Table 1

Wayne State Experimental Data

Species	Resultant Acceleration, g's	Intracranial Pressure Increase, kPa	Pathology
Human Cadaver	160	241-276	Skull Fracture
Stumptail Monkey	2100	276	Skull Fracture
Rhesus Monkey	1550	345-517	Concussion
	2100	—	Skull Fracture
Canine	900-1100	310	Concussion
	1200-1300	517	Skull Fracture

Note. The mass of the striker for each case was 0.86kg. Impact energies ranged from 73.8 to 87.9J as impact velocities increased from 13.1 to 14.3$\frac{m}{s}$. A dash indicates that the intracranial pressure increase was not obtained.

The researchers scaled the head sizes for each of the canine and sub-human primate test subjects in relation to the head sizes for the postmortem human subjects to demonstrate a relationship between the skull fractures in the human subjects against skull fractures and concussions in the animal subjects. The researchers used this information combined with previously published prevalence data suggesting that there was an occurrence of skull fracture in approximately 78 to 80 percent of adult human concussions to determine concussion for a given combination of acceleration and intracranial pressure increases due to direct impact. This combination of information led the researchers at Wayne State to set a scaled value of 80 to 90 g's of acceleration lasting four milliseconds (ms) and having a time-to-maximum acceleration, also known as rise time, of between 1 and 1.5ms to be the critical level in predicting concussion for

the adult healthy normal population (Gurdjian, 1975). The Wayne State model was used as a standard by many subsequent researchers in the development of injury tolerance equations although it was found to be inaccurate for indirect impacts and was based on many assumptions regarding the mechanical and geometric properties of the human head (Mertz & Patrick, 1993).

The early research by Gadd at General Motors, and Gurdjian and coworkers at Wayne state led to the development of a tolerance model in 1971 which was labeled the Head Injury Criterion. The model extended the initial work of Gadd by confining the acceleration measurement to only the initial linear head acceleration caused by an impact. The equation for the Head Injury Criterion had a critical injury threshold value similar to the Gadd Severity Index, but removed the estimated acceleration due to rebound, which was included in Gadd's initial estimate. Although the Head Injury Criterion still lacked the ability to predict level of injury, it was established as the reference standard for the automotive sector and athletic equipment manufacturers in North America.

In a report for the Society of Automotive Engineers, Versace discussed how the head impact tolerance models created by Gadd and the Wayne State researchers, in 1966 and 1971 respectively, were effective based on the body of knowledge that was available to them at the time. Unfortunately, magnitude of linear acceleration was not the only danger experienced by the head due to direct impact (Versace, 1993). Mechanical engineers have long understood that small forces operating at a distance off center causes more physical damage than much larger forces acting directly through the center of mass. This is attributed to the mechanical property termed torque, which in

the case of head impact causes rotational acceleration of the head and neck resulting in shear forces (Beer & Johnston, 1976; Brands, Bovendeerd, & Wismans, 2002). Through accident reconstruction researchers discovered that it was rare to have only a single form of head acceleration, which was exclusively linear or exclusively rotational. The influence of each acceleration form and the combination of the accelerations on injury outcome are still under debate (Chinn, Canaple, Derler, Doyle, Otte, Schuller, et al., 2001). In a 2003 study, however, King et al showed that linear acceleration caused a resulting brain motion in the order of one millimeter (±0.001m) compared with angular acceleration induced brain motion of five millimeters (±0.005m). Additionally, brain motion due to angular acceleration was not reduced through the use of a helmet (Hoshizaki & Brien, 2004; King et al., 2003).

Studies by the European Commission Directorate General for Energy and Transport attempted to understand potential head injury due to impact. The tolerance models evolved to better explain the dramatic effect of rotation on the head (Chinn et al., 2001; Versace, 1993). A Generalized Acceleration Model for Brain Injury Tolerance, or GAMBIT, was developed through a combination of automotive crash reconstructions and their associated hospital records. This model accounted for both linear and rotational acceleration, direct and indirect impacts, and was relatively accurate in predicting the severity of injury outcome. The original GAMBIT has undergone many revisions, but the model now uses measured maximal linear and rotational accelerations to calculate a moving threshold value for multiple levels of injury (Chinn et al., 2001).

Many other factors have been investigated for relevance in head injury prediction, including elastic skull deformation, individual cranial geometry, and history of concussion (Babbs, 2006). In addition, the frequency of vibration caused by impact has been suggested to affect the brain differently at distinct levels and has been recognized as an area that requires further investigation (Chinn et al., 2001). These earlier studies are fundamental to the understanding of head impacts leading to concussive symptoms. Most notably, the information gained from head injury tolerance curves have provided an essential foundation in understanding the effect of different types of impacts (Versace, 1993).

This research thesis was composed of two studies. The first study was a pilot investigation to show evidence of the validity and reliability of the instruments and methodology used in the second, main investigation. The principal investigation explored the possible expansion of head injury tolerance curve information based on vibration and the frequency domain of impacts in order to improve predictive models. The frequency domain uses a mathematical transform to change time domain measures of time and acceleration in the abscissa and ordinate to frequency and power of vibration (Smith, 2002).

Delimitations

The scope of this study was delimited to:

1. The use of a spherical cast urethane headform with high biofidelity was used to represent the human head. It was assumed the head would react in a similar manner without endangering human participants or requiring postmortem human subjects.

2. The inclusion of two drop heights, 0.2m and 0.4m. Heights used in helmet testing of greater than one meter would be unnecessarily high for testing with an unhelmeted headform and would result in extreme impacts.
3. The inclusion of direct impacts only. Indirect causes of head acceleration, such as body impacts causing the type of injuries often associated with whiplash, were not considered in this study.

Limitations

The following limitations were identified:

1. The headform was constructed of cast urethane and may not possess the same level of biofidelity that is now standard on instruments currently used in helmet testing such as the Hybrid III anthropometric test device or similar models. This limitation did not affect the validity of outcomes from the present study; however results may not be generalized to live subject head injury prediction models. Differences among headforms have been noted by researchers with respect to relevance of impact measurement comparison between studies and testing procedures (Bishop, Norman, & Kozey, 1984).
2. The headform was not free to rotate; therefore, angular measures were extrapolated from kinematic and kinetic equations.
3. Mechanical wear to the Headform Impact Measurement Device and headform was expected to occur, however, the impact of this deformation was accepted to be minimal and inconsequential to the study's outcome.
4. Due to the manual release of the mechanical switch supporting the headform, minor errors in drop height were present. These drop height variances were kept

within one millimeter (±0.001m) and were not expected to affect the study's dependent measures significantly.

REVIEW OF LITERATURE

Head Trauma

Mild traumatic brain injury, also referred to as cerebral concussion, currently lacks a single definition. Numerous classification systems have been developed, often with only subtle differences in delimiting factors, in order to quantify the immediate and lingering effects of the brain injury (Cantu, 2001).

The 2nd International Symposium on Concussion in Sport was held in 2004, and outlined five common features to be used in defining the nature of a concussive head injury (McCrory, Johnston, Meeuwisse, Aubry, Cantu, Dvorak, et al., 2005). For historical purposes it is important to understand the basis of such grading systems; however it is now generally accepted that these are no longer clinically relevant with respect to duration of symptoms. Degree of severity and the ability to recover is highly individualized and return to normal function is dictated solely on the disappearance of symptoms.

An example of such a classification system is the Evidence-Based Cantu Grading System for Concussion. On Cantu's grading scale, a mild or grade 1 concussion was defined by posttraumatic retrograde and anterograde amnesia or postconcussion signs or symptoms lasting less than 30 minutes. No loss of consciousness was associated with a mild concussion. Grade 2 or moderate concussions were characterized by loss of consciousness lasting less than one minute. Additionally, moderate concussions were identified by posttraumatic retrograde and anterograde amnesia or postconcussion signs or symptoms lasting longer than 30 minutes but less than 24 hours. Grade 3, the most severe level of concussion according

to Cantu was classified by a loss of consciousness lasting more than one minute or posttraumatic retrograde and anterograde amnesia lasting longer than 24 hours. Postconcussion signs or symptoms lasting longer than 7 days were also deemed to be distinguishing symptoms of a grade 3 concussion (Cantu, 2001).

An alternative to Cantu's classification system is the Abbreviated Injury Scale (AIS), which defines seven levels of head injury from uninjured, through minor, moderate, serious, severe, critical, and finally, maximum or untreatable. This system is commonly used to rank head injuries of all forms including concussions, skull fractures, and cervical fractures (Chinn et al., 2001).

The impact of head injuries on society has been explored by multiple researchers as they are the most common severely disabling injuries in the United States (Guskiewicz & Mihalik, 2006). In a study, conducted in 1985 by Frankowski, Annegers, and Whitman reported that approximately five hundred thousand new cases occur annually and although most of these were classified as mild traumatic brain injuries, 30-50 percent were moderate to fatal head injuries (Frankowski, Annegers, & Whitman, 1985). In 1993 a similar study was published by Kraus (as cited in Babbs, 2006) which reported nearly two million persons seeking medical treatment with head injury annually in the United States. Kraus also found that three hundred thousand of those treated were hospitalized with approximately a third of those suffering severe head injury on the Abbreviated Injury Scale, resulting in prolonged coma, permanent neurological impairment, or death (Babbs, 2006). After Frankowski et al's findings, the United States Department of Health and Human Services reported that for those who sustained severe but sub-fatal head impacts, the cost for the first year of direct health care was

310 000 USD per injury (United States Department of Health and Human Services, 1989).

Cognitive deficits and an increase in re-injury probability were two frequently investigated results of head trauma. Multiple aspects of attention were altered namely impaired reaction response, reduced concentration ability, slowed information processing, and decreased performance on memory tasks (Gronwall, 1991). Gronwall also stated that there was evidence from studies of amateur boxers that repeated head trauma resulted in more severe attention deficits. Similarly, Moser and Schatz identified an enduring effect of repeated head injury due to direct head impact trauma in an adolescent population with respect to academic achievement (Moser & Schatz, 2002). A prospective cohort study of incidence and risk factors for head trauma injury in adolescent athletes by Schultz et al found that the risk of concussion more than doubled among the athletes with previously recorded concussions (Shultz, Marshall, Mueller, Yang, Weaver, Kalsbeek, et al., 2004).

Many head injury researchers have suggested that a preventative approach may be the most suitable method to avoid future injuries and reduce healthcare costs. This preventative healthcare model requires a better understanding of head injury causation. With better knowledge of injury mechanism and injury tolerance equations it may become possible to develop better protective devices, in the form of helmets, or to establish more comprehensive rules in sport. Research which focuses on the biomechanics of head impacts should provide information to help prevent injuries (Guskiewicz & Mihalik, 2006).

Impact Testing

Test Design

Headdrop procedures are frequently used in the evaluation of helmet impact attenuation (Caswell & Deivert, 2002) or the capacity of a helmet to protect. One of the primary North American models for this type of testing is administered by the National Operating Committee on Standards for Athletic Equipment (NOCSAE) headquartered in the United States, although several other testing protocols exist including the Canadian Standards Association (CSA) and American Society for Testing and Materials (ASTM). For the purpose of the current study, a modified NOCSAE protocol and test device was implemented. The stated purpose of the NOCSAE testing standard is to specify "basic performance requirements, methods, and equipment used for testing protective headgear" (National Operating Committee on Standards for Athletic Equipment, 2007). Individual performance standards for impact velocities, pass/fail criteria and other performance requirements are specified in individual standard specifications depending on the sport (National Operating Committee on Standards for Athletic Equipment, 2007). NOCSAE requires six categories of information to be recorded while using their procedure, namely the name and location of the test laboratory; name of laboratory technician; model, manufacturer, manufacture date, and size of each headgear tested; observed temperature in each conditioning and testing environment; impact results incorporating the impact locations, drop height, severity index, and peak acceleration; and the testing date (NOCSAE, 2007). Neither duration of impact, nor impact angle are measured in the NOCSAE impact test, although both have been identified as critical factors in the identification of head trauma severity (Versace, 1993; Gennarelli, 1993).

Similarly, impact acceleration frequency is not tested through the NOCSAE standard, which has been suggested as a contributing element to the proper understanding of impact outcome (Babbs, 2006). Additionally, in the NOCSAE drop test, the headform was connected to a zero compliance neck structure, which eliminated the ability of the system to rotate either before or after contact. This lack of rotation limited the testing protocol to only direct and linear impacts (NOCSAE, 2007).

Another deleterious scenario associated with impact to the top or top boss locations of the head was the injurious effect to the neck. Previous research has determined that impacts directed through the top of the head, even when the head was protected with a helmet, caused injuries to the neck associated with the load on the cervical spine (Bishop & Wells, 1990). This cause of neck injury was not well defined through the NOCSAE drop test as the relative stiffness of the neck to the helmet was a critical factor in injury prediction (Bishop & Wells, 1990).

In comparison to the North American standard, European head-drop testing protocols allow for a headform to drop in freefall. Freefall drops allow for a completely compliant system at contact, allowing the headform to rotate in any direction as a result of the external force imparted by the strike plate. This too was not a representative model, as the human head and neck complex is not compliant to this extreme level (Chinn et al., 2001).

Tolerance Criteria

One of the primary objectives of studying head injury biomechanics is to determine appropriate tolerance criteria to identify the probability of brain injury or skull fracture (Versace, 1993). The concept of a head injury criterion taking anything more

than maximum acceleration into account was first developed from the Wayne State Tolerance Curve in 1971, which plotted linear acceleration magnitude versus durations of three to five milliseconds. The data for the curve was derived from laboratory impacts to postmortem human subjects causing skull fracture and sub-fracture concussive impacts to a very limited number of anaesthetized primates and canines (Goldsmith, 1981). Current North American head injury criteria standards, such as the Gadd Severity Index in Equation 1 or the Head Injury Criteria (HIC) in Equation 2, are based solely on the translational acceleration experienced by the head and the time the acceleration is experienced. Neither North American model accounts for any rotational component to head acceleration. Of interest is the similarity between the Gadd Severity Index (GSI) equation in Equation 1 and the standard equation for impulse in Equation 3. The Gadd Severity Index uses the instantaneous acceleration expressed as a multiple of acceleration due to gravity in the place of force. Since force is proportional to mass and acceleration, Gadd has essentially discounted the effect of mass on the prediction of injury. Gadd assumed that the weighted impulse of head impact acceleration was sufficient in the determination of head injury outcome. The Head Injury Criterion weights the Gadd Severity Index with a time to maximum acceleration factor, although the relatively untested threshold value and exponential weight remain the same at 1 000 and 2.5, respectively (Lockett, 1985). These primarily North American criteria, do not account for any head rotation (Versace, 1993; Lockett, 1985).

$$GSI = \int_{t_1}^{t_2} \vec{A}^{2.5} dt \tag{1}$$

Where, $\vec{A}$ is the instantaneous acceleration expressed as a multiple of $\vec{g}$;

dt are the increments of time in seconds;

t_1 *to* t_2 is the essential duration of the acceleration pulse;

and if GSI ≥ 1 000, the head impact conditions are unacceptable. (Gadd, 1993)

$$HIC = (t_2 - t_1)\left[\frac{1}{(t_2 - t_1)}\int_{t_1}^{t_2} \vec{A}dt\right]^{2.5} \quad (2)$$

Where, $\vec{A}$ is the instantaneous acceleration expressed as a multiple of g;

dt are the increments of time in seconds;

t_1 *to* t_2 is the essential duration of the acceleration pulse;

and if HIC ≥ 1 000, the head impact conditions are unacceptable. (Lockett, 1985)

$$Impulse = \int_{t_1}^{t_2} \vec{F}dt \quad (3)$$

Where, $\vec{F}$ is the instantaneous force acting on the particle;

dt are the increments of time in seconds;

t_1 *to* t_2 is the essential duration of the applied force; (Beer & Johnston, 1976)

It has been suggested that rotational acceleration may be considerably more damaging to the brain, when compared to purely linear acceleration, due to shear forces experienced during head rotation (Lighthall, Melvin, & Ueno, 1993). In addition to differences between translational and rotational acceleration, the point of application of acceleration, as well as the axis of rotation have been shown to influence the severity of

brain injury in adult sub-human primates (Gennarelli, Thibault, Tomei, Wiser, Graham, & Adams, 1993).

More recently, an evolving series of equations called the Generalized Acceleration Model for Brain Injury Tolerance, or GAMBIT, have attempted to account for both translational and rotational acceleration with respect to potential brain injury. The original version of GAMBIT, as expressed by Newman, was a function as shown in Equation 4, which assumed that a translational acceleration of 250g's and a rotational acceleration of 10 000 $\frac{rad}{s^2}$ were critical cut-off values regarding brain injury. If a value of 1 or higher is returned from Newman's formula, with respect to a measured head impact, a head injury of some level was predicted to have occurred.

$$G(t) = \left[\left(\frac{\vec{a}(t)}{\overrightarrow{a_c}}\right)^m + \left(\frac{\vec{\alpha}(t)}{\overrightarrow{\alpha_c}}\right)^n\right]^{1/s} \tag{4}$$

Where, $G(t)$ is the instantaneous measure of interest with a threshold value of 1;

$\vec{a}(t)$ is the instantaneous linear acceleration at time t;

$\vec{\alpha}\ (t)$ is the instantaneous rotational acceleration at time t;

$\overrightarrow{a_c}$ is the critical value for linear acceleration;

$\overrightarrow{\alpha_c}$ is the critical value for rotational acceleration;

m, n, and s are empirical constants set to match the data set;

For a linearly weighted model, the constants are set to 1;

For an elliptical model, the constants are set to 2.

(Sances, Larson, Yoganandan, & Pintar, 2000)

This model was later modified in order to account for the maximum accelerations, instead of instantaneous measures. Through experimentation on rhesus monkeys, Lee developed a GAMBIT equation that predicted the occurrence of a traumatic acute subdural hematoma due to high shear strain. Lee discovered that the two forms of acceleration, namely linear and rotational, could be combined in different percentages to cause the same head injury outcome. Lee's simplified GAMBIT is shown in Equation 5.

$$GAMBIT = 4\overrightarrow{a_m} \times 10^{-4} + 8\,\overrightarrow{\propto_m} \times 10^{-3} \quad (5)$$

Where, $GAMBIT$ is the measure of interest with a threshold value of 1;

$\overrightarrow{a_m}$ is the maximum linear acceleration;

$\overrightarrow{\propto_m}$ is the maximum rotational acceleration.

(Sances, Larson, Yoganandan, & Pintar, 2000)

This model was further refined by Kramer and Appel in 1990, when they used an extensive field accident database to define more accurate human critical values of 250g's and 25 000 $\frac{rad}{s^2}$ for translational and rotational accelerations, respectively. The researchers were also able to determine a more suitable value of 2.5 for the three empirical constants through the 18 000 motorcycle accident reconstructions. Kramer and Appel's final mathematical model is shown in Equation 6.

$$GAMBIT = [(4\overrightarrow{a_m} \times 10^{-3})^{2.5} + (4\ \overrightarrow{\propto_m} \times 10^{-5})^{2.5}]^{1/2.5} \quad (6)$$

Where, $GAMBIT$ is the measure of interest with threshold values associated with the Abbreviated Injury Scale;

$\overrightarrow{a_m}$ is the maximum linear acceleration;

$\overrightarrow{\propto_m}$ is the maximum rotational acceleration.

(Sances, Larson, Yoganandan, & Pintar, 2000)

Additionally, the Abbreviated Injury Scale (AIS) was linked by the researchers to the GAMBIT (Chinn et al., 2001). A series of risk curves, with GAMBIT score as the abscissa and the probability of sustaining the level of injury as the ordinate, allowed for the prediction of injury severity based on the maximum translational and rotational acceleration imparted to a head (Sances, Larson, Yoganandan, & Pintar, 2000). This predictive approach is graphically represented in Figure 1, Head Injury Severity Probability as a Function of GAMBIT.

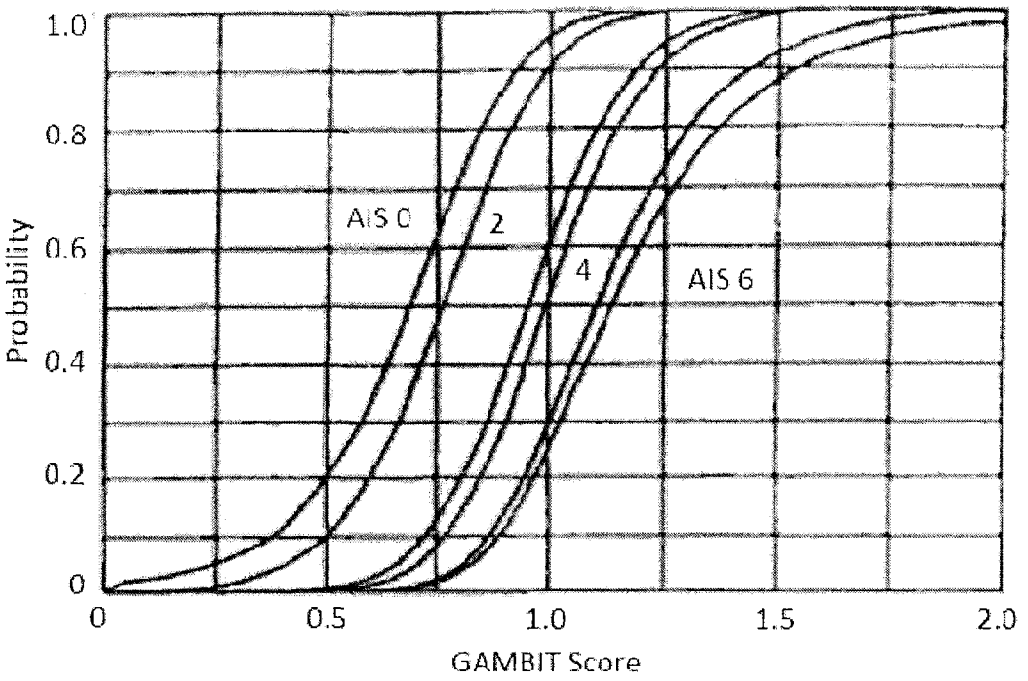

Figure 1. Head Injury Severity Probability as a Function of GAMBIT

Therefore, if a head impact had linear and rotational accelerations that determined a GAMBIT score of 0.5, the subject had approximately an eighty percent chance of sustaining no head injury and a ten percent chance each of suffering a mild or moderate head injury. If the impact was more severe and the calculated GAMBIT increased to 1.5, the subject would have roughly a ninety percent chance of being untreatable and a five percent chance each of obtaining a severe or critical head injury. It should be noted that if the GAMBIT were a perfect prediction model, the threshold curves would be straight vertical lines with solely discrete responses. As this was not the case, either insufficient quantities of data have been obtained with the current factors or there was an additional predictive factor to be added to the model.

A similar method of injury severity prediction was attempted with the Head Injury Criterion as shown in Figure 2, with original conclusions being that a score of greater

than 1 500 related to an injury level of moderate or above on the Abbreviated Injury Scale (Got et al., 1993). This supposition was not supported due to the large number of high Head Injury Criterion scores with no recorded injury.

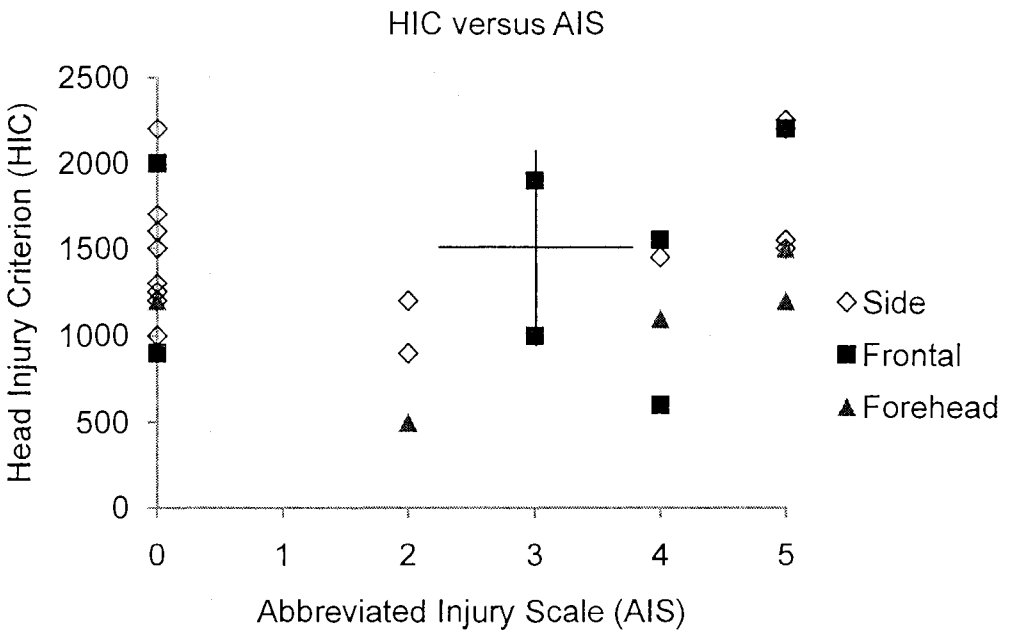

Figure 2. HIC versus AIS (Got et al., 1993)

In order to use the GAMBIT effectively, both linear and rotational acceleration data must be analyzed from an impact. Unfortunately, although this information is available in laboratory testing, it is rare to have measured data from a field setting (Cisco, Chu, Greenwald, 2004). Methods for the determination of impact location and angle, which allow for the calculation of rotational acceleration in conjunction with linear acceleration measures, have been developed with moderate field success. Namely, a method was developed at the Wayne State University Biomechanics Research Center based on measurement of angular acceleration of a rigid body using linear accelerometers. This method allowed for accurate measurement within a head impact laboratory environment (Padgaonkar, Krieger, & King, 1975). A nine accelerometer set

was found to be accurate in predicting resultant head acceleration within approximately five percent under low impact accelerations. The error value was ten times higher under high impact accelerations (Padgaonkar, Krieger, & King, 1975). The theories developed at Wayne State were altered by Simbex LLC, a biomechanics company associated with Dartmouth College in New Hampshire, into a field system for the estimation of acceleration magnitude and impact location using multiple linear accelerometers. Average error rates in the field system were reported as ten percent under normal conditions (Crisco, Chu, & Greenwald, 2004). Similar error results were reported by Biokinetics and Associates Ltd. in their reconstruction of American football collisions from a field accelerometer system (Newman, Beusenberg, Shewchenko, Withnall, & Fournier, 2005). This technological approach represented a large leap forward in the ability to quantify head injury in a field setting (Duma et al., 2005); however the level of error remained undesirably high.

Multiple studies have shown that frequency domain analysis of biomechanical data can yield more useful information than commonly selected time domain data analysis (Clancy, Farina, & Merletti, 2005; White, Agouris, & Fletcher, 2005). In a clinical analysis of gait patterns for children with cerebral palsy, White et al investigated the benefit of including fundamental frequency, as well as other frequency domain factors, in the categorization of gait symmetry using a series of force platforms. The researchers discovered that the inclusion of frequency domain factors with already implemented time domain factors significantly improved the ability to quantify gait patterns (White et al., 2005). This research was a clinical continuation of theories presented by Antonsson and Mann who analyzed the frequency content of gait

(Antonsson & Mann, 1985). A cross-comparison of time and frequency domain methods in the analysis of multiple hand-grip tasks was conducted in 2005 by Clancy, Farina, and Merletti. The researchers found that the inclusion of both time and frequency domain factors proved beneficial in describing hand dynamometer measures. Also of note from their research was the finding that frequency domain factors did improve with longer sampling times (Clancy, Farina, & Merletti, 2005). Chinn et al have suggested that the principles examined by others with respect to frequency domain analysis of biomechanical data could be transferred to the analysis of head impacts.

Although research related to improving the technology used to measure linear and angular accelerations is ongoing (Yoganandan, Zhang, Pintar, & Liu, 2006), as has been presented (Chinn et al, 2001) investigation of head impact frequency may help reduce the effect of error associated with field design and improve prediction using the GAMBIT and Head Injury Criterion.

METHODOLOGY AND PROCEDURES

Purpose

The purpose of the present study was to evaluate the drop height, headform orientation, and location of an impact based on specific time and frequency domain factors recorded in perpendicular and tangential headform impacts.

Objectives

The present study was designed to meet the following objectives:

To investigate the relationship between fundamental frequency, head acceleration, and center of pressure measures recorded in perpendicular and tangential impacts when using a headform in guided free fall.

To investigate the extent to which fundamental frequency, high to low frequency ratio, vertical force, headform acceleration and center of pressure measures can be used to identify the height, orientation, and location of a headform impact.

Pilot Investigation

Assessing the Reliability and Validity of the Instruments

Purpose

An initial pilot study was conducted to determine estimates of reliability and validity for the modified Headform Impact Measurement Device. The pilot study addressed the following three objectives:

Objectives

To investigate the relationship between vertical acceleration measures from the modified Headform Impact Measurement Device and the vertical force measures from the Advanced Mechanical Technologies, Inc force platform.

To determine the inter-reliability of measurement response, with respect to vertical acceleration magnitude and frequency, for the modified Headform Impact Measurement Device.

To determine the statistical power based on drop quantity, specifically comparing the use of twenty trials to one hundred trials.

To determine the intra-reliability of measurement response, with respect to vertical acceleration magnitude and frequency, for the modified Headform Impact Measurement Device.

Instruments

Headform Impact Measurement Device. The original Headform Impact Measurement Device was based on the Canadian Standards Association (CSA) helmet testing equipment. The device, shown in Figure 3, measured eighty centimetre (0.80m) and was constructed at Lakehead University through collaboration between the faculties of Kinesiology and Engineering (Marsh, 2007). A triaxial accelerometer was placed at the center of mass of a five kilogram (5kg) headform with a sensitive axis aligned to within five degrees (5°) of vertical. The triaxial accelerometer uses a small piezoelectric acceleration transducer with three orthogonal axes. It was designed to measure vibration in three mutually exclusive axes. The headform was connected to a vertical low-friction rail, extending from the top of the device inferiorly to a point seventeen centimetres (0.17m) above the bottom plate, to allow for standardized drops.

The cast urethane headform was designed to approximate the mass and size of an adult human head at five kilograms and 0.61 meters in circumference about the reference plane. The headform had a neck with zero compliance so that the path of the

head while falling was linear. After release, the headform fell along the vertical low-friction rail solely as a result of gravity.

The headform struck a polytetrafluoroethylene (PTFE) plate measuring 0.10 meters in diameter and 0.023 meters in height, with a tensile strength of 26.89 MPa and a durometer reading of D50 on the shore hardness scale. This hardness value approximated the impact that would be sustained against a hockey helmet. The strike plate then mechanically transferred the impact through a 0.010 meter aluminium disk into an AMTI force platform.

The vertical mono-rail track on the original Headform Impact Measurement Device was extended inferiorly to the bottom plate to guard against the headform derailing under dynamic impact conditions. The strike plate at the center of the bottom plate was reduced in height and reinforced to reduce unwanted vibrations within the device. The Modified Headform Impact Measurement Device was securely fastened to an AMTI force platform in a manner that minimized vibration between the two measurement tools.

AMTI force platform. An AMTI force platform fitted with four load cells (exterior dimensions 0.508, 0.464, and 0.0826m, respectively) was used to quantify forces and moments being applied to its surface. Foil strain gages were attached to each of the load cells to form six Wheatstone bridges, with three of the output voltages indicating the proportional level of force in the three axes and the remaining three indicating the measured amount of moment about each of the axes. The force platform was designed to be firmly mounted to a rigid surface for optimal linearity and minimal crosstalk.

Upper limits for platform loading were calculated based on Equation 9 within Appendix C, which accounted for force in each of the axes, the moment about the vertical axis, and the location of the load on the surface of the platform (Advanced Mechanical Technology, Inc, 1987).

Glockenspiel. A wooden based Sonor Percussion Glockenspiel with metal keys, capable of producing frequencies ranging from 261.5Hz to 698.5Hz. The glockenspiel was firmly fixed with tape to the AMTI force platform during the testing procedures.

Analog-to-digital converter. A PowerLab analog-to-digital converter manufactured by ADInstruments was selected for the testing procedures. The converter was capable of handling 400 000 samples per second over eight analog input channels. The converter received analog voltage inputs and transformed the signal into a digital output. The converter then transferred the digitized signal to a computer at up to 840 megabits per second through a USB 2.0 cable. The stated accuracy of the PowerLab analogue-to-digital converter was better than 0.1%; with both zero and gain drift compensation integrated within the unit (ADInstruments Pty Ltd., 2006).

Experimental Tasks

The procedures for the pilot investigation were designed to address each of the four pilot study objectives. The Headform Impact Measurement Device was tested for validity and reliability under multiple scenarios in order to fine-tune the machine and testing protocol. The unhelmeted headform was dropped from various heights under a variety of conditions.

The modified Headform Impact Measurement Device was securely bolted to an AMTI force platform with the top of the head aligned with the positive axis for $\overrightarrow{F_y}$ and the

negative axis for $\overrightarrow{F_x}$ on the platform. The headform was oriented for a front impact site and the strike plate was placed in the primary location. Five tasks were completed in the testing of the force platform and the modified Headform Impact Measurement Device.

Task 1 assessed the reliability of two release techniques. A total of two hundred drops were assessed at a drop height of 0.40m. Half of the drops were conducted using a mechanical switch, while the other half was released manually. The vertical force means and standard deviations for the two groups were $\bar{x}$ = 6.6755, *SD* = 0.7451 and $\bar{x}$ = 6.7285, *SD* = 0.8544, respectively. A comparison of the two groups showed no significant difference with $t(199) = 0.6409$ (two-tailed), therefore since the drops using the mechanical switch showed less variability the switch was selected as the method of release.

Task 2 compared the reliability of measurements using a PTFE strike plate to not using the strike plate. Another one hundred drops were preformed using the mechanical switch release but no strike plate. The mean of 6.8353 and standard deviation of 0.9231 were compared to the values recorded in Task 1. A two-tailed t-test showed no significant difference between the groups with $t = 0.3967$. As before, with less variability was recorded using the strike plate, the use of the strike plate was accepted.

Concurrent validity of the triaxial accelerometer was assessed with respect to the force platform in Task 3. Three drops each were preformed from forty different drop heights ranging from 0.02 to 0.80 meters. No significant differences were found between odd and even trial block groups established in the data, with a *t*-score of 0.8290.

Task 4 investigated the sampling strategy with respect to drop quantity. A random sampling of groups consisting twenty, forty, sixty, eighty, and one hundred drops were compared. No significant differences were found between any of the groups. In order to minimize mechanical degradation of the headform and modified Headform Impact Measurement Device, it was established that twenty drops would be used for each subsequent testing group.

Frequency recognition was assessed in task 5. Thirteen different known frequencies, ranging from 261.5 to 698.5 Hertz were created on the force platform. The frequencies were measured and the known frequencies were compared to the measured frequencies. No differences were recorded between the expected and observed frequencies. This suggested that the device was valid in measuring frequency.

Additional information regarding the pilot investigation is documented in Appendix B of the present study.

Instruments

The principal research investigation utilized the same instrumentation as the pilot investigation, with the exception of the Headform Impact Measurement Device. The Modified Headform Impact Measurement Device was used due to its superior ability to withstand repeated dynamic headform impacts as compared to the original device.

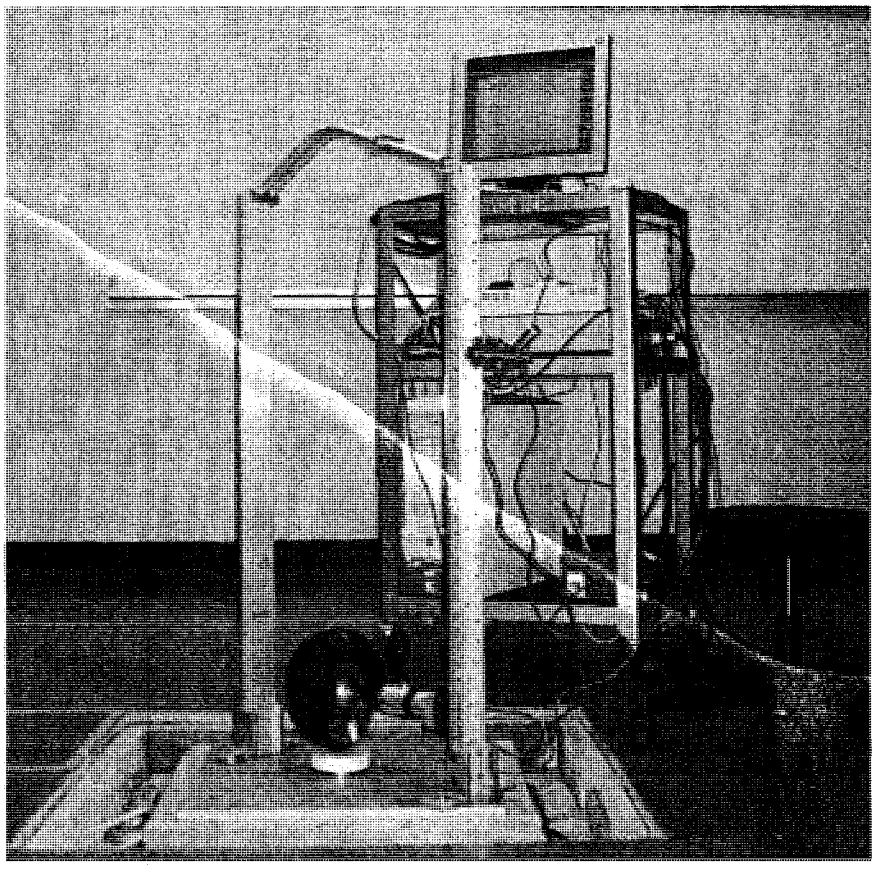

Figure 3. Instrument Design

All voltage measures from the force platform were received by an AMTI amplifier before all six channels; $\overrightarrow{F_x}$, $\overrightarrow{F_y}$, $\overrightarrow{F_z}$, $\overrightarrow{M_x}$, $\overrightarrow{M_y}$, and $\overrightarrow{M_z}$, respectively, were sent through a PowerLab 8/30 analog-to-digital converter. The PowerLab was an instrument manufactured by ADInstruments, designed to convert analog signals such as force platform or accelerometer voltage into a digital signal which was then processable by a computer. The voltage signal from the accelerometer passed through a separate amplifier with unity gain before entering the same PowerLab converter as channel seven. An eighth channel was used as a trigger to separate trials. The trigger circuit was created, as illustrated in Figure 4, Toggle Switch Schematic, giving an output of 4.5V when the toggle switch was pressed.

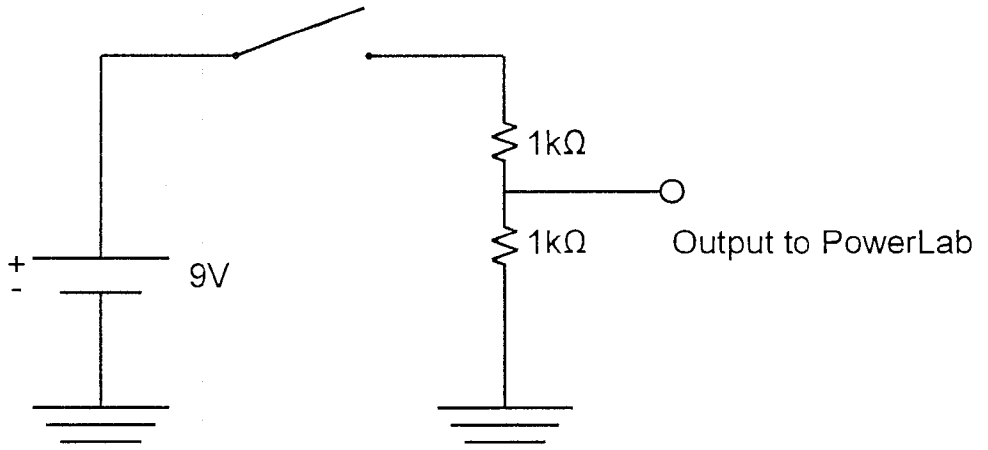

Figure 4. Toggle Switch Schematic

From the PowerLab converter, the eight channels were captured simultaneously via USB through the PowerLab Chart 5 software. A threshold voltage of three volts in channel eight indicated the beginning of each new trial and prompted the software to begin a simultaneous timed capture of four seconds for all eight channels. The complete testing diagram is shown in Figure 5.

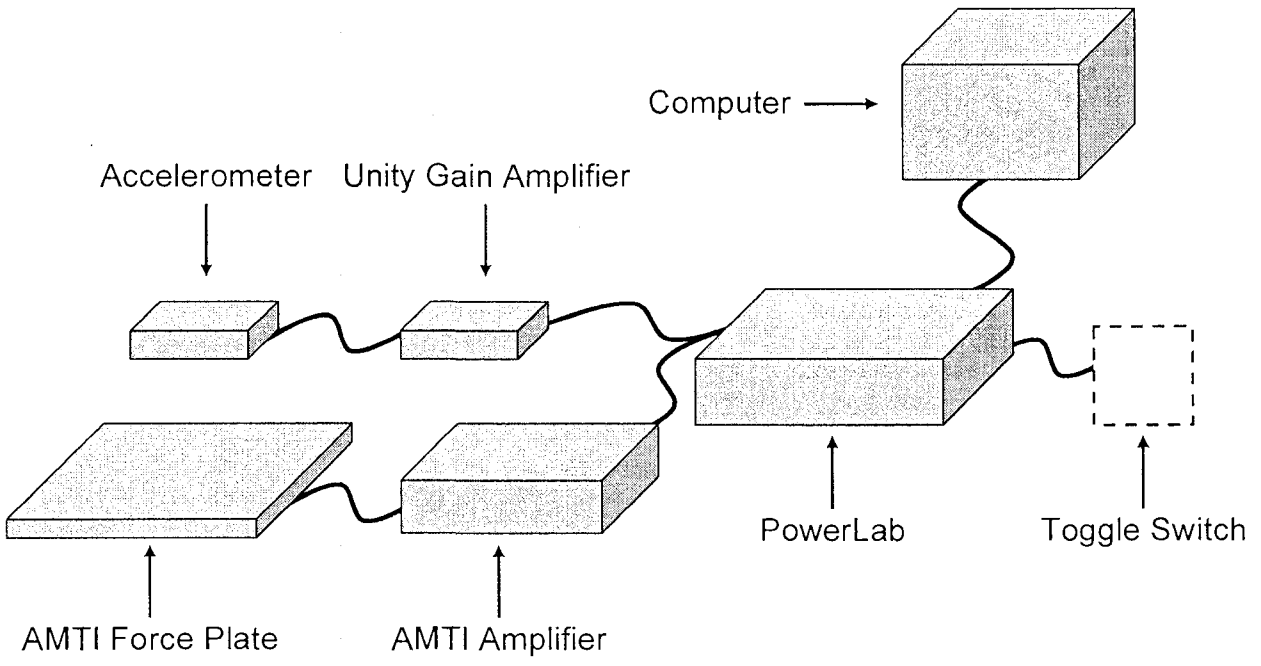

Figure 5. Testing Schematic

Headform Impact Measurement Device Procedures

Due to the maximum drop height of eighty centimeters (0.80m) and an unhelmeted headform, a modified version of the National Operating Committee on Standards for Athletic Equipment (NOCSAE) calibration protocol for drop testing was implemented. An unhelmeted headform was dropped from incrementally increasing heights standardized to 0.20 and 0.40 meters onto six impact sites. These two drop heights equate to impact energies of 9.8 and 19.6 Joules, respectively, as shown in Appendix E. These impact energies were analogous to values used in the testing of shell geometry attenuation characteristics (Spyrou, 1997). More than one drop height was necessary in order to increase the measurement variability and therefore strengthen the data analysis. The impact locations were termed front, front boss, side, rear boss, rear, and top boss marked as F, FB, S, RB, R, and TB, respectively, as illustrated in Figure 6 and Figure 7 (National Operating Committee on Standards for Athletic Equipment, 2007). These headform impacts simulated direct perpendicular and tangential head impacts in each of the six locations. Acceleration to the head caused by indirect contact, such as a whiplash injury, were not included in this study.

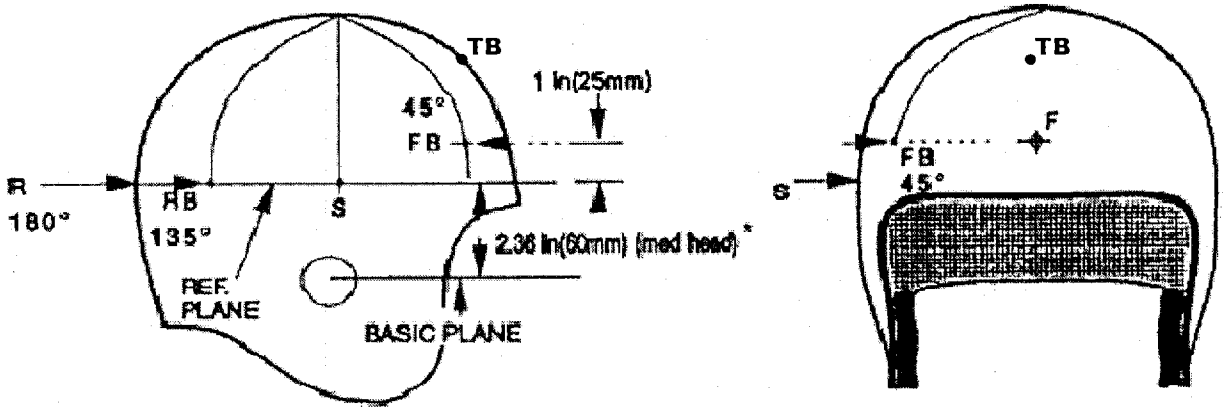

Figure 6. Impact Sites (NOCSAE, 2007)

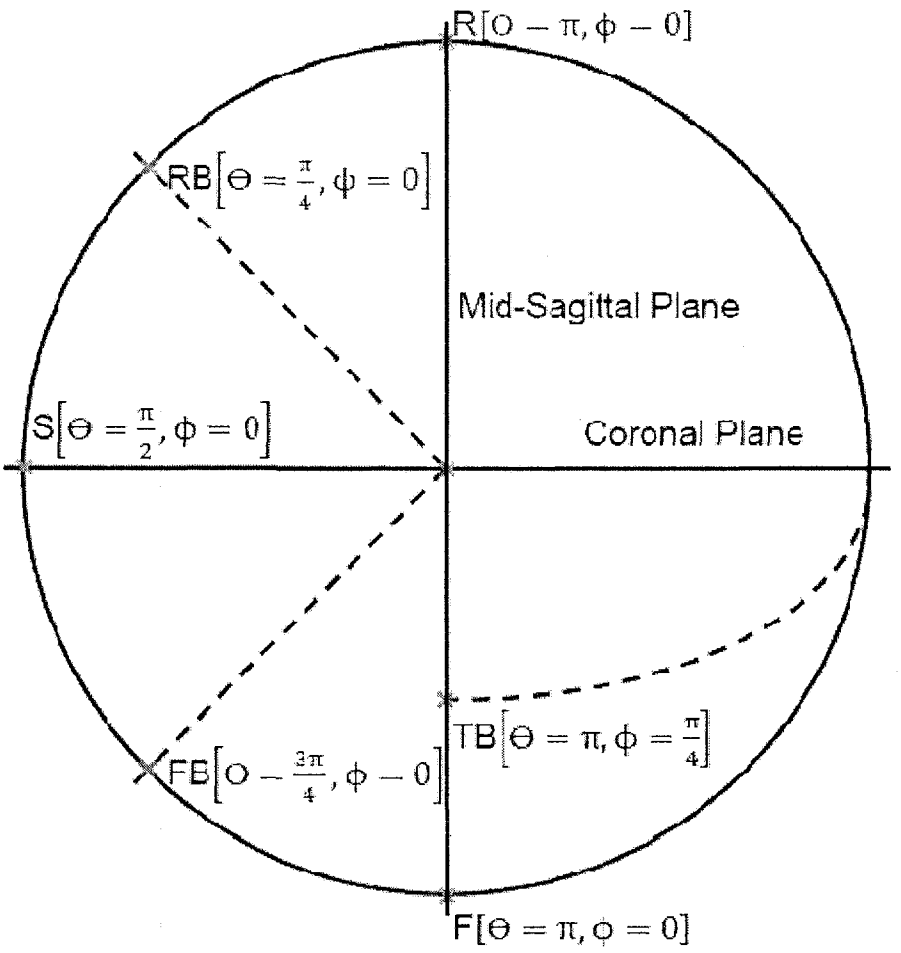

Figure 7. Superior View of Headform

Center of pressure measures from the AMTI force platform were calculated in order to establish the baseline distance off center for the impacts. Equations used to calculate these values were taken from embedded functions within AMTI software as illustrated in Equation 7, Center of Pressure Equations. This correlate of torque was later used to compare values recorded during perpendicular and tangential impacts to the headform.

$$\vec{X} = \frac{-(\overrightarrow{M_y} - \vec{Z} \times \overrightarrow{F_z})}{\overrightarrow{F_z}} \quad (7)$$

$$\vec{Y} = \frac{(\overrightarrow{M_x} - \vec{Z} \times \overrightarrow{F_y})}{\overrightarrow{F_z}}$$

Where, $\overrightarrow{M_y}$ is the moment or torque about the Y axis;

$\overrightarrow{M_x}$ is the moment or torque about the X axis;

$\overrightarrow{F_y}$ is the force in the Y axis;

and $\overrightarrow{F_z}$ is the force in the vertical Z axis. (AMTI, 1990)

Measures of Perpendicular Orientation

The procedures for perpendicular drops began with the selection of an appropriate physical space in which to conduct the testing. The laboratory had controllable lighting, minimal audible noise, and as little floor vibration as possible. Access to the laboratory was restricted throughout the testing in order to minimize variability.

In order to ensure consistency, the laboratory temperature, humidity, and elevation remained constant; the mass of the headform was not altered and each of the measurement tools were securely fastened to one another. Laboratory conditions were measured and reported. Ambient lighting, which was registered by the force platform as vibration occurring at 60Hz and the associated harmonics, was kept to a minimum and constant level. These precautions were in place to minimize signal noise from the system.

Drop heights were standardized to 0.2 and 0.4 meters for each impact site. The headform was not spherical and therefore, the distance from the strike plate to the

vertical center of the headform changed based on the headform rotation. Since the vertical center of the headform was the reference point for drop height measurement, differences in baseline position was taken into account. Table 2 represents the standardization measurements for the perpendicular drop height locations based on impact site.

Table 2

Perpendicular Drop Height Standardization

	Drop Height (m)		
Impact Site	0.200	0.400	Baseline
Front	0.720	0.520	0.920
Front Boss	0.728	0.528	0.928
Side	0.740	0.540	0.940
Rear Boss	0.725	0.525	0.925
Rear	0.720	0.520	0.920
Top Boss	0.726	0.526	0.926

Note. Baseline measurements were taken with the headform resting on the PTFE strike plate. The two drop height measurements were assessed off of the Baseline data.

Measures of Tangential Orientation

The second stage of the study followed a similar testing pattern to the first stage. An unhelmeted headform was dropped from progressively increasing heights of 0.20 and 0.40 meters. Impact measures were recorded from both an AMTI force platform and a triaxial accelerometer mounted within a headform. The difference in the testing protocol was the location of the strike plate, which was offset from center in the coronal plane by 0.05 meters for each of the impact sites. This strike plate location was termed

the tangential position. The headform was aligned as before in the perpendicular impacts.

In moving the strike plate, the baseline measurements for drop height were altered due to the strike plate making contact at a different angle to the headform. Similar to Table 2, the values shown in Table 3 standardized the measurements for the tangential drop height locations based on impact site.

Table 3

Tangential Drop Height Standardization

	Drop Height (m)		
Impact Site	0.200	0.400	Baseline
Front	0.720	0.520	0.920
Front Boss	0.728	0.528	0.928
Side	0.740	0.540	0.940
Rear Boss	0.730	0.530	0.930
Rear	0.719	0.519	0.919
Top Boss	0.726	0.526	0.926

Note. Baseline measurements were taken with the headform resting on the PTFE strike plate. The two drop height measurements were assessed off of the Baseline data.

The variables that were measured for comparison between unhelmeted perpendicular and tangential contacts were the magnitude and the frequency of the impact accelerations, based on the AMTI force platform and the triaxial accelerometer. Any significant differences between the two types of impacts were noted and analyzed.

Definition of Variables

Raw Data

Linear acceleration in the vertical axis experienced by the acceleration transducer within the headform was denoted as $\vec{a}$ and was measured in Volts.

The force platform measured both forces and moments related to each of the three axes. These six variables of $\overrightarrow{F_x}$, $\overrightarrow{F_y}$, $\overrightarrow{F_z}$, and $\overrightarrow{M_x}$, $\overrightarrow{M_y}$, $\overrightarrow{M_z}$, respectively, were all measured in Volts.

None of the acceleration, force, or moments was converted to real world units because of the potential error term introduced when calculating the direct scaling factor based on a measured known weight. Since the data analysis used in the present study was not altered by the variable units, the use of raw voltage data was possible.

Calculated Data

The $\vec{X}$ and $\vec{Y}$ center of pressure values were calculated according to the equations in Equation 7. Subsequently, the Pythagorean Theorem was implemented in order to identify the third dependent variable of average resultant displacement off of center, represented by $\vec{D}$.

Represented by f_F, the fundamental frequency of the impact accelerations was measured from the frequency spectrum's first harmonic, which is typically the first maximal peak after the signal passes the low frequency noise. In the case of this study, the frequency with the highest power from the fast-Fourier transform was equivalent to the fundamental frequency. This held true due to the dramatic difference in power scale between the noise of the system and the impact measurement. This variable had units of Hertz or cycles per second.

After a threshold frequency was established at the median frequency recorded of 250Hz, all frequencies below the threshold were labeled as low frequency and those above the cut-off as high frequency. A ratio of high to low frequency was then calculated and represented as f_R. This ratio effectively eliminated the influence of signal noise because the testing conditions were kept constant for each trial and the comparison of ratios included the same noise for each trial.

Data Analysis

Smoothing

Before the raw voltage signals from the force platform were converted into digital signals by the PowerLab converter, the voltages were processed by the AMTI amplifier, which performed two functions. The first function that the amplifier completed was a physical filter. In this study, the low-pass filter was set to allow any signals below 1050Hz. Any signal above this cut-off was considered to be signal noise. The second function of the amplifier was to apply signal gain, or to amplify the signal strength. Gain was calculated by the ratio of signal out to signal in, therefore, an original voltage signal from the Modified Headform Impact Measurement Device was said to be multiplied by the given value for gain before continuing on to the analogue-to-digital converter. The gain for the vertical force, $\overrightarrow{F_z}$, was set to 1 000 and all other channels for the force platform were set to a gain of 4 000.

Similarly, the raw voltage signal from the accelerometer within the Modified Headform Impact Measurement Device passed through a unity gain amplifier before the signal was processed by the analogue-to-digital converter. This isolated the relatively low impedance electric circuit for the accelerometer from the potentially high impedance circuit for the analogue-to-digital converter. Unity gain amplifiers have a gain of one, therefore the magnitude of raw voltage in was equal to the voltage signal out.

Voltage values were not smoothed or filtered within the Chart5 software for this study.

Statistical Approach

The statistical approach for this study consisted of three categorical variables, namely impact site, drop height, and headform orientation. These variables were predicted and were denoted as S, H, and O, respectively. There were also five measured variables included in the design, namely vertical force, linear acceleration, center of pressure displacement, fundamental frequency, and frequency ratio denoted as $\vec{F}$, $\vec{a}$, $\vec{D}$, f_F, and f_R, respectively. For each combination of the categorical variables, each measured variable was tested and recorded twenty times as outlined in the pilot investigation. Maximum values were used for the subsequent analysis, similar to Lee and Kramer and Appel's Generalized Acceleration Models for Brain Injury Tolerance.

The data collected in this study was normally distributed and the variance between groups was homogeneous. A model using a series of discriminant functions to identify the categorical variables was therefore appropriate for this analysis. The present study had a conglomerate function which represented the combined outcome for impact site, drop height, and headform orientation. The number of discriminant functions used for each level of the series was equal either to the number of predictors or the number of possible categorical outcomes minus one, whichever was less. If more than one function was required to identify the possible outcomes at a given level, the first function maximized the between group separation. Each subsequent function was uncorrelated to the previous function or functions and further separated the groups as much as possible (Diekhoff, 1992).

Model Comparison

Two discriminant function prediction models were created and compared. The first model used only measured time domain factors in calculating estimates of the categorical variables. This model was termed the frequency domain exclusion model and is shown in Equation 8.

$$\delta_E = C_{S(l,k,j)} - (C_{O(k,j)} - (C_{H(j)} - (\beta_{1(l,k,j,i)}\overrightarrow{F_z} + \beta_{2(l,k,j,i)}\vec{a} + \beta_{3(l,k,j,i)}\vec{D} + K_{(l,k,j,i)}) \quad (8)$$

Where, δ_E is the error term;

$C_{S(l,k,j)}$is the centroid for impact site with iteration (l, k, j);

$C_{O(k,j)}$is the centroid for headform orientation with iteration (k, j);

$C_{H(j)}$is the centroid for drop height with iteration (j);

(i) is the function iteration with 1, 2, 3;

(j) is the iteration for drop height with 1 [0.2m], 2 [0.4m];

(k) is the iteration for headform orientation with 1 [perpendicular], 2 [tangential];

(l) is the iteration for impact site with 1 [F], 2 [FB], 3 [S], 4 [RB], 5 [R], 6 [TB];

$\vec{a}$ is the measured acceleration of the headform;

$\overrightarrow{F_z}$ is the measured vertical force on the force platform;

$\vec{D}$ is the calculated center of pressure displacement;

$\beta_{x(l,k,j,i)}$ is the canonical coefficient associated with a factor and iteration;

$K_{(l,k,j,i)}$ is a canonical constant associated with an iteration;

and when $\delta_E = 0$, the iteration numbers for (j), (k), and (l) identify the drop height, headform orientation, and impact site, respectively.

The second model incorporated both time and frequency domain factors and was called the frequency domain inclusion model. The frequency domain inclusion model is represented as Equation 9.

$$\delta_I = C_{S(l,k,j)} - (C_{O(k,j)} - (C_{H(j)} - (\beta_{1(l,k,j,i)}\overrightarrow{F_z} + \beta_{2(l,k,j,i)}\vec{a} + \beta_{3(l,k,j,i)}\vec{D} + \beta_{4(l,k,j,i)}f_F + \beta_{5(l,k,j,i)}f_R + K_{(l,k,j,i)}) \quad (9)$$

Where, δ_I is the error term;

$C_{S(l,k,j)}$is the centroid for impact site with iteration (l,k,j);

$C_{O(k,j)}$is the centroid for headform orientation with iteration (k,j);

$C_{H(j)}$is the centroid for drop height with iteration (j);

(i) is the function iteration with 1, 2, 3, 4, 5;

(j) is the iteration for drop height with 1 [0.2m], 2 [0.4m];

(k) is the iteration for headform orientation with 1 [perpendicular], 2 [tangential];

(l) is the iteration for impact site with 1 [F], 2 [FB], 3 [S], 4 [RB], 5 [R], 6 [TB];

$\vec{a}$ is the measured acceleration of the headform;

$\overrightarrow{F_z}$ is the measured vertical force on the force platform;

$\vec{D}$ is the calculated center of pressure displacement;

f_F is the fundamental frequency in Hertz;

f_R is the ratio of high to low frequencies;

$\beta_{x(l,k,j,i)}$ is the canonical coefficient associated with a factor and iteration;

$K_{(l,k,j,i)}$ is a canonical constant associated with an iteration;

and when $\delta_I = 0$, the iteration numbers for (j), (k), and (l) identify the drop height, headform orientation, and impact site, respectively.

By comparing the two models using a *z* test for proportion, it was possible to identify the effective predictability change when including the frequency domain factors as opposed to excluding the factors. Predictability was defined as a ratio of correct predictions to total cases. This model comparison was calculated for each categorical variable prediction outcome.

RESULTS

This chapter was divided into four sections. First, the drop test descriptive statistics were outlined for each of the four subcategories. Next, this was followed by presentation of the unstandardized canonical discriminant functions, function centroids, and determination of the predictability for two models both including and excluding frequency domain factors. Decision trees for both models highlighted the series of unstandardized canonical discriminant functions implemented for greater predictability outcomes. The model including frequency domain factors was compared to the model that only used time domain factors based on ability to predict. Finally, additional drop tests were assessed using the two models and the accuracy levels of prediction were demonstrated.

Descriptive Statistics

In Table 4, the means and standard deviations were provided for the four subcategories created by the combination of headform orientation, perpendicular versus tangential, and drop heights of 0.2 and 0.4 meters. The total number of drops was 480, with each subcategory consisting of n = 120 drop tests and having an equal prior probability.

Table 4

Descriptive Statistics for Drop Tests

Variable	Headform Orientation			
	Perpendicular		Tangential	
	$\bar{x}$	*SD*	$\bar{x}$	*SD*
	0.2m			
Force in the Vertical Axis	5.223	0.706	4.600	0.631
Headform Acceleration	0.432	0.149	0.296	0.096
Center of Pressure Displacement	1.399	0.357	1.164	0.347
Fundamental Frequency	109.091	17.103	100.285	7.751
Frequency Ratio	2.421	0.695	3.280	1.149
	0.4m			
Force in the Vertical Axis	6.778	0.890	6.473	0.892
Headform Acceleration	0.568	0.246	0.501	0.185
Center of Pressure Displacement	0.895	0.426	0.508	0.320
Fundamental Frequency	114.966	17.541	104.810	7.748
Frequency Ratio	2.974	0.459	3.335	0.686

Note. $N = 480$. $n = 120$ for each group.

For each of the dependent variables larger values were observed for the 0.4m drop height compared to the 0.2 meter drop height, as illustrated in Table 4. Likewise, a similar trend was observed for the mean and standard deviation for each of the variables, force in the vertical axis, headform acceleration, center of pressure displacement, and fundamental frequency for perpendicular versus tangential impact

orientations. This trend was reversed for frequency ratio, indicating either more high frequency or less low frequency components in tangential impacts. Table 5 demonstrates the significant difference found between the groups, for each of the variables presented in Table 4. All of the measured variables showed significant differences between groups at the $p < 0.001$ level.

Table 5

Analysis of Variance for Drop Tests

Variable	*F*	Significance
Force in the Vertical Axis	204.786	$p < 0.001$
Headform Acceleration	51.084	$p < 0.001$
Center of Pressure Displacement	132.296	$p < 0.001$
Fundamental Frequency	26.075	$p < 0.001$
Frequency Ratio	33.920	$p < 0.001$

Note. N = 480. *df* = 479.

The results of a Tukey's post hoc test applied to the drop test subcategories showed that the only two group sets that did not differ significantly were the 0.2m perpendicular and 0.4m tangential fundamental frequency at $p = 0.065$ and 0.2m and 0.4m tangential frequency ratio with $p = 0.948$. The distinct nature of the measured variables supported the use of each measured variable in a discriminant analysis because the group means were used to differentiate between groups.

Prediction Models

Predictive unstandardized canonical discriminant functions were created based on measured variables for both a model including and a model excluding frequency

domain factors. Drop height, headform orientation, and impact site were all predicted using a series of three groups of functions. Each function used only variables that met the inclusion criteria of a stepwise selection method using an *F* to enter value of 3.84 (Diekhoff, 1992) for that individual analysis. Initially all measured variables were excluded from the functions and the Wilks' Lambda for each variable was calculated. The variable that minimized the Wilks' Lambda, or the ratio of error to effect variance, was included in the analysis if it had an *F* value greater than the *F* to enter threshold. This process was repeated with the remaining variables until the variable that minimized Wilks' Lambda did not exceed the *F* to enter threshold. Any measured variables that were excluded in the final function were given a weighting coefficient of zero. From the functions, group centroids were calculated representing the average value for the weighted variables. Lastly, a category was predicted based on centroid proximity.

Frequency Domain Inclusion Prediction Model

The decision tree in Figure 8 below illustrates the series of functions used based on determinations made at an earlier point on the hierarchy. Each of the functions included all three traditional measured time domain factors, both measured frequency domain factors, and a constant. Drop height was assessed first. The calculated value for height was then compared to the function centroids and was predicted to either be 0.2 or 0.4 meters. Based on the predicted height assessed from the function coefficients and centroids displayed in Table 6, the functions from either Table 7 or Table 8 were used to predict headform orientation as either perpendicular or tangential. Finally, impact site was predicted using the appropriate equations from Table 9 to Table 12.

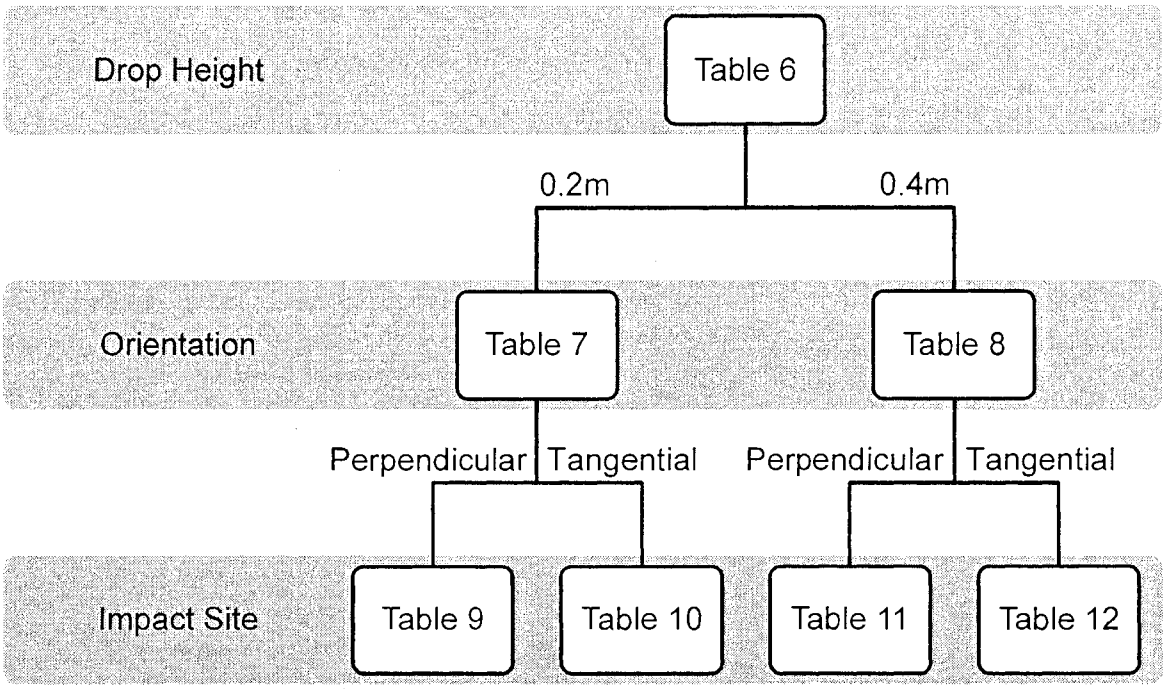

Figure 8. Frequency Domain Inclusion Decision Tree

Tables 11 through 17 present the *F* to enter, unstandardized canonical discriminant coefficients, and group centroids for the five measured variables force in the vertical axis, headform acceleration, center of pressure displacement, fundamental frequency, and frequency ratio. The total number of drop tests was 480, however the sample size was halved between Table 7 and Table 8 for $n = 240$ each. This sample size was halved again for the next level on the Frequency Domain Inclusion Decision Tree, leaving sample sizes of $n = 120$ for each of Tables 9 through 12.

Table 6

Height Canonical Discriminant Coefficients

Variable	*F* to Enter	Coefficients
Force in the Vertical Axis	519.422	1.139
Headform Acceleration	35.768	1.774
Center of Pressure Displacement	32.853	-1.091
Fundamental Frequency	3.947	0.008
Frequency Ratio	215.827	0.771
Constant		-9.486
Functions at Group Centroids		
0.2m		-1.582
0.4m		1.582

Table 7

Orientation Canonical Discriminant Coefficients at 0.2m

Variable	F to Enter	Coefficients
Force in the Vertical Axis	60.554	1.214
Headform Acceleration	69.596	5.150
Center of Pressure Displacement	29.556	1.511
Fundamental Frequency	1.961[a]	0
Frequency Ratio	0.531[a]	0
Constant		-9.773
Functions at Group Centroids		
Perpendicular		0.906
Tangential		-0.906

[a]Did not meet the *F* to Enter threshold value of 3.84 and was excluded from the canonical prediction function.

Table 8

Orientation Canonical Discriminant Coefficients at 0.4m

Variable	*F* to Enter	Coefficients
Force in the Vertical Axis	0.623[a]	0
Headform Acceleration	0.811[a]	0
Center of Pressure Displacement	63.328	1.965
Fundamental Frequency	8.820	0.026
Frequency Ratio	32.756	-1.050
Constant		-0.888
Functions at Group Centroids		
Perpendicular		0.701
Tangential		-0.701

[a]Did not meet the *F* to Enter threshold value of 3.84 and was excluded from the canonical prediction function.

Table 9

Impact Site Canonical Discriminant Coefficients at 0.2m Perpendicular

Variable	*F* to Enter	Function 1	2	3	4
		Coefficients			
Force in the Vertical Axis	19.538	1.396	-0.939	-0.036	2.259
Headform Acceleration	3.288[a]	0	0	0	0
Center of Pressure Displacement	13.317	3.098	0.924	-2.468	1.041
Fundamental Frequency	17.030	0.041	0.032	0.053	-0.017
Frequency Ratio	5.026	-0.176	0.535	0.391	2.340
Constant		-15.674	-1.187	-3.056	-17.090
Functions at Group Centroids					
Front		-0.708	0.223	-0.657	-0.492
Front Boss		-1.069	-0.713	0.563	-0.513
Side		2.342	0.331	0.572	-0.212
Rear Boss		0.804	-0.173	-0.989	0.165
Rear		-1.219	1.115	0.309	0.351
Top Boss		-0.150	-0.784	0.201	0.701

[a]Did not meet the *F* to Enter threshold value of 3.84 and was excluded from the canonical prediction functions.

Table 10

Impact Site Canonical Discriminant Coefficients at 0.2m Tangential

Variable	*F* to Enter	Function 1	2	3	4
		Coefficients			
Force in the Vertical Axis	11.549	1.059	0.636	1.135	-0.361
Headform Acceleration	2.499[a]	0	0	0	0
Center of Pressure Displacement	7.769	1.128	-1.392	2.091	1.400
Fundamental Frequency	22.961	0.054	-0.025	-0.049	-0.021
Frequency Ratio	5.939	1.714	2.532	0.024	0.857
Constant		-19.485	-7.749	-3.951	1.056
Functions at Group Centroids					
Front		-1.000	-0.666	0.778	0.118
Front Boss		0.246	0.395	0.218	-0.077
Side		2.407	-0.242	-0.295	0.091
Rear Boss		-0.521	-1.013	-0.441	-0.139
Rear		-1.421	0.672	-0.747	0.092
Top Boss		0.289	0.853	0.487	-0.084

[a]Did not meet the *F* to Enter threshold value of 3.84 and was excluded from the canonical prediction functions.

Table 11

Impact Site Canonical Discriminant Coefficients at 0.4m Perpendicular

Variable	*F* to Enter	Function 1	2	3
		Coefficients		
Force in the Vertical Axis	4.942	2.576	1.701	-0.658
Headform Acceleration	3.469[a]	0	0	0
Center of Pressure Displacement	8.841	2.905	1.392	2.288
Fundamental Frequency	3.047[a]	0	0	0
Frequency Ratio	9.878	0.382	1.458	-0.065
Constant		-16.483	-14.228	0.574
Functions at Group Centroids				
Front		-0.103	0.214	0.231
Front Boss		1.331	-0.284	-0.034
Side		0.751	0.127	0.118
Rear Boss		-1.371	-0.751	0.048
Rear		-0.734	0.945	-0.108
Top Boss		0.126	-0.251	-0.255

[a]Did not meet the *F* to Enter threshold value of 3.84 and was excluded from the canonical prediction functions.

Table 12

Impact Site Canonical Discriminant Coefficients at 0.4m Tangential

Variable	*F* to Enter	Function 1	2	3	4	5
		Coefficients				
Force in the Vertical Axis	28.458	1.325	0.696	0.602	-0.173	-0.843
Headform Acceleration	21.763	3.910	-5.491	1.547	2.906	1.288
Center of Pressure Displacement	14.183	4.350	0.863	-1.057	-2.396	1.251
Fundamental Frequency	4.070	0.014	0.072	-0.034	0.118	0.029
Frequency Ratio	5.771	-0.211	0.801	1.596	-0.124	0.220
Constant		-13.452	-12.447	-5.945	-11.066	0.400
Functions at Group Centroids						
Front		-1.392	0.036	0.213	-0.473	0.003
Front Boss		1.928	0.646	-0.260	0.367	0.002
Side		1.360	0.908	0.225	-0.223	-0.003
Rear Boss		-2.341	-0.139	-0.784	-0.009	-0.001
Rear		-2.276	-0.239	0.600	0.400	-0.001
Top Boss		2.722	-1.212	0.008	-0.063	-0.001

The effectiveness of the predictive unstandardized canonical discriminant functions using a combination of time and frequency domain factors is illustrated in Table 13 as a ratio of correct predictions to total cases. The functions were more accurate in determining both headform orientation and impact site for the lower drop

height of 0.2 meters. Additionally, the tangential impact sites were predicted correctly more frequently than the perpendicular sites.

Table 13

Frequency Domain Based Determination Predictability

Variable	Selection Basis	Level	Prediction Ratio
Height			0.944
Orientation	Height	0.2m	0.825
		0.4m	0.754
		Mean	0.790
Impact Site	Height & Orientation	0.2m Perpendicular	0.600
		0.2m Tangential	0.608
		0.4m Perpendicular	0.367
		0.4m Tangential	0.592
		Mean	0.542

Note. Prediction Ratio was the ratio of correct predictions to total cases.

Frequency Domain Exclusion Prediction Model

Similar to Figure 8, the Frequency Domain Exclusion Decision Tree illustrates the series of functions used based on determinations made at an earlier point on the decision hierarchy. For this analysis, each of the functions included only the three traditionally measured time domain factors and a constant. As presented previously with the prediction method using frequency domain factors, drop height was predicted initially. The calculated value for height was then compared to the function centroids from Table 14 and the trial was predicted to either be 0.2 or 0.4 meters. Based on the

predicted height, the functions and centroids from either Table 15 or Table 16 were used to predict headform orientation as either perpendicular or tangential. Finally, impact site was predicted using the appropriate equations from Table 17 to Table 20.

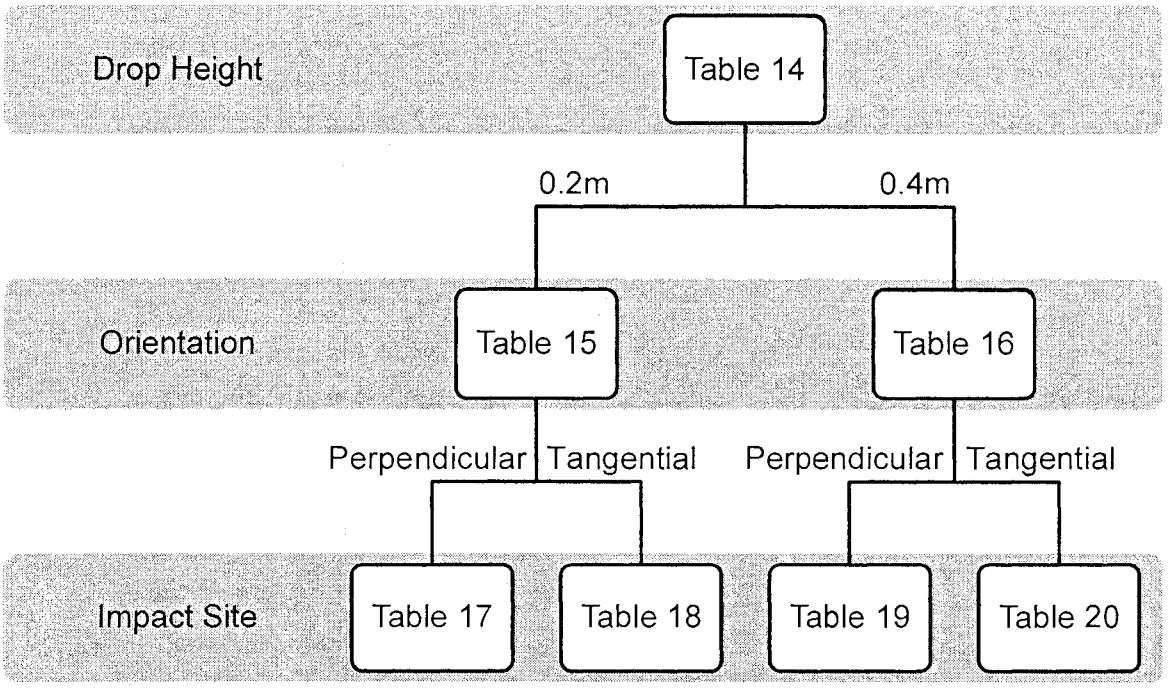

Figure 9. Frequency Domain Exclusion Decision Tree

Mirroring the information presented in Tables 6 through 12, Tables 14 through 20 present the *F* to enter, unstandardized canonical discriminant coefficients, and group centroids. Only the time domain measured variables of force in the vertical axis, headform acceleration, and center of pressure displacement were included in the model presented in this section. The total number of drop tests was $N = 480$, sample size was halved for each level on the Frequency Domain Exclusion Decision Tree, leaving sample sizes of $n = 240$ and $n = 120$ for Tables 15 through 16 and Tables 17 through 20, respectively.

Table 14

Height Canonical Discriminant Coefficients

Variable	*F* to Enter	Coefficients
Force in the Vertical Axis	519.442	0.817
Headform Acceleration	63.015	2.410
Center of Pressure Displacement	86.353	-1.483
Constant		-4.325
Functions at Group Centroids		
0.2m		-1.335
0.4m		1.335

Table 15

Orientation Canonical Discriminant Coefficients at 0.2m

Variable	*F* to Enter	Coefficients
Force in the Vertical Axis	60.554	1.214
Headform Acceleration	69.956	5.150
Center of Pressure Displacement	29.556	1.511
Constant		-9.773
Functions at Group Centroids		
Perpendicular		0.906
Tangential		-0.906

Table 16

Orientation Canonical Discriminant Coefficients at 0.4m

Variable	*F* to Enter	Coefficients
Force in the Vertical Axis	13.963	0.535
Headform Acceleration	0.021[a]	0
Center of Pressure Displacement	63.328	2.580
Constant		-5.353
Functions at Group Centroids		
Perpendicular		0.581
Tangential		-0.581

[a]Did not meet the *F* to Enter threshold value of 3.84 and was excluded from the canonical prediction function.

Table 17

Impact Site Canonical Discriminant Coefficients at 0.2m Perpendicular

		Function	
		1	2
Variable	*F* to Enter	Coefficients	
Force in the Vertical Axis	14.355	1.884	-0.969
Headform Acceleration	3.347[a]	0	0
Center of Pressure Displacement	22.169	3.617	2.046
Constant		-14.902	2.196
Functions at Group Centroids			
Front		-0.470	0.585
Front Boss		-1.049	-0.861
Side		1.594	0.009
Rear Boss		1.178	0.388
Rear		-1.387	0.712
Top Boss		0.135	-0.833

[a]Did not meet the *F* to Enter threshold value of 3.84 and was excluded from the canonical prediction functions.

Table 18

Impact Site Canonical Discriminant Coefficients at 0.2m Tangential

		Function	
		1	2
Variable	*F* to Enter	Coefficients	
Force in the Vertical Axis	9.571	1.136	0.811
Headform Acceleration	2.869[a]	0	0
Center of Pressure Displacement	6.553	2.809	-1.195
Constant		-10.215	-4.425
Functions at Group Centroids			
Front		0.318	-0.127
Front Boss		0.134	0.247
Side		1.163	-0.215
Rear Boss		-0.220	-0.292
Rear		-1.572	-0.071
Top Boss		0.177	0.459

[a]Did not meet the *F* to Enter threshold value of 3.84 and was excluded from the canonical prediction functions

Table 19

Impact Site Canonical Discriminant Coefficients at 0.4m Perpendicular

Variable	*F* to Enter	Function 1	Function 2	Function 3
		Coefficients		
Force in the Vertical Axis	9.026	1.973	-0.522	-0.625
Headform Acceleration	3.952	3.275	10.993	1.216
Center of Pressure Displacement	7.365	2.145	-1.686	2.196
Constant		-12.542	1.108	-0.041
Functions at Group Centroids				
Front		-0.276	-0.415	0.195
Front Boss		1.282	-0.450	-0.085
Side		0.889	0.538	0.190
Rear Boss		-1.229	-0.152	-0.012
Rear		-0.911	0.276	-0.044
Top Boss		0.245	0.202	-0.244

Table 20

Impact Site Canonical Discriminant Coefficients at 0.4m Tangential

		Function		
		1	2	3
Variable	*F* to Enter	Coefficients		
Force in the Vertical Axis	28.458	1.405	0.481	0.886
Headform Acceleration	21.763	3.787	-6.374	-0.710
Center of Pressure Displacement	14.183	4.366	2.166	-1.841
Constant		-13.208	-1.023	-4.441
Functions at Group Centroids				
Front		-1.313	0.193	-0.085
Front Boss		1.849	0.385	0.091
Side		1.395	0.702	0.032
Rear Boss		-2.412	0.209	-0.103
Rear		-2.211	-0.627	0.152
Top Boss		2.692	-0.861	-0.088

Prediction outcomes for the frequency domain exclusion model are presented in Table 21 with the results from the subcategories calculated from Tables 19 through 25 represented as a ratio of correct predictions to total trials. A general trend was present of drops from 0.2m being more accurately predicted, with the exception of 0.4m tangential drops being properly classified roughly seven percent more often than 0.2m tangential trials.

Table 21

Time Domain Based Determination Predictability

Variable	Selection Basis	Level	Prediction Ratio
Height			0.915
Orientation	Height	0.2m	0.825
		0.4m	0.679
		Mean	0.752
Impact Site	Height & Orientation	0.2m Perpendicular	0.525
		0.2m Tangential	0.400
		0.4m Perpendicular	0.367
		0.4m Tangential	0.467
		Mean	0.439

Note. Prediction Ratio was the ratio of correct predictions to total cases.

Model Comparison

To compare the predictability of the two models, a *z* test for proportion was used to determine if the statistical difference between the prediction ratio between the frequency domain inclusion and exclusion models was significant. As shown in Table 22 below, the frequency domain inclusion model was significantly more effective than the frequency domain exclusion model at predicting each discriminant category.

Table 22

Model Determination Predictability Comparison

Variable	Prediction Ratio by Model		*z*	*p*
	Exclusion	Inclusion		
Height	0.915	0.944	2.763	$p < 0.01$
Orientation	0.752	0.790	2.044	$p < 0.05$
Impact Site	0.439	0.542	4.485	$p < 0.01$

Secondary Data Analysis

Twenty additional drops were analyzed using both the frequency domain inclusion and frequency domain exclusion models for each impact site of front, side, and rear at both 0.2 and 0.4 meters. The unstandardized canonical discriminant functions from Table 9, Table 10, Table 17, and Table 18 that were derived from primary data were assessed with secondary data that was not used in the creation of the functions. The results from this analysis are presented in Table 23.

Table 23

Secondary Data Analysis

Coefficient Location	Prediction Ratio by Data		*z*	*p*
	Primary	Secondary		
	Frequency Domain Inclusion Model			
Table 9	0.600	0.600	0	1.0000
Table 10	0.367	0.350	0.273	0.7847
	Frequency Domain Exclusion Model			
Table 17	0.525	0.550	-0.388	0.6982
Table 18	0.400	0.350	0.790	0.4292

Note. None of the secondary test data sets were significantly different from the primary model data sets.

DISCUSSION

The results from the previous chapter were related to existing literature on headform impacts and the two stated objectives of the current study. The primary purpose of the present study was to investigate the extent to which fundamental frequency, high to low frequency ratio, vertical force, head acceleration and center of pressure measures could be used to identify the height, orientation, and location of a headform impact in guided free fall. Upon initial inspection, with three categorical variables S, H, and O, and five measured variables $\vec{F}$, $\vec{a}$, $\vec{D}$, f_F, and f_R a logistic regression could be used to analyze the significant difference among groups. Logistic regression is the most commonly used statistical method to differentiate prediction outcomes. Two of the main assumptions of the logistic regression are that the data is not normally distributed and that the variance between groups is not homogeneous. Since the data collected in this study was normally distributed and variance between groups was homogeneous, as evident from the descriptive statistics presented in the results chapter, a model using a series of discriminant functions to identify the categorical variables was more appropriate. Through the application of a discriminant analysis model which included frequency domain factors versus a model which excluded frequency domain factors, it was possible to identify the influence of the frequency domain factors in improving predictability outcomes for headform impacts.

Results from the four subcategories of the initial 480 headform impacts followed predictable patterns. Larger measures and greater standard deviations related to both the higher drop height and the perpendicular headform alignment for four of the five factor variables. A discrepancy for the latter condition with the frequency ratio variable

indicated that the balance of high to low frequencies was affected differently from the other variables between perpendicular and tangential impacts.

Within this study, a model's inability to predict outcomes properly was a result of two possible reasons. First, if there were an insufficient number of trials collected, factor weights could not be sufficiently refined (Lockett, 1985). The second scenario for inaccurate discriminant prediction occurs if an influential factor was not considered in the model. Referring back to the plot of GAMBIT score versus AIS in Figure 1, it was evident from the derived curvilinear thresholds that the information collected from 18 000 trials could not uniquely discriminate injury severity level. As the number of trials used to establish the GAMBIT was substantial, it was suggested that a necessary predictive factor was still missing from the GAMBIT calculation (Chinn et al., 2001). This deficiency in injury prediction might be at least partially rectified through integration of frequency domain information into the calculation of the GAMBIT. Based on the initial findings from the present study, this concept of including frequency domain factors to further describe direct head impact could also be extended to the HIC or GSI. The potential shift in injury severity plots with the inclusion of frequency domain factors represents a possible refinement of existing head injury criteria.

For the current study, the frequency domain inclusion model implemented two novel frequency domain factors, fundamental frequency and frequency ratio. Additionally, two measured time domain factors describing the linear motion of the headform and one calculated time domain factor indicating the rotational motion were included in the drop height, headform orientation, and impact site prediction

calculations. These time domain factors were force in the vertical axis, headform acceleration, and center of pressure displacement, respectively.

When measuring head impact through traditional methods, researchers consider signal noise experienced by linear accelerometers to be high as a result of local vibration. Heavy filters and smoothing have been shown to drastically reduce the ability of linear accelerometer sets to predict angular acceleration of the head (Yoganandan et al., 2006). Frequency domain measures may allow for true signal recognition from linear accelerometers without excessive data smoothing. In particular, a ratio of high to low frequencies standardized the signal noise effectively reducing the mathematical influence of the noise on the frequency domain as shown in the present study's inclusion model. The technique of splitting the frequency spectrum into low and high portions was similar to a method commonly used in electromyography analysis where researchers have shown that when the frequency spectrum was split into two parts they can separate the contributing influences to muscle contraction. For example, in work reported by Ebenbichler et al, the authors suggested that by splitting the frequency spectrum at the median frequency they were able to more accurately describe muscle contraction (Ebenbichler, Bonato, Roy, Lehr, Posch, Kollmitzer, et al., 2002).

The frequency domain inclusion model was unique in its approach to quantify headform impacts. Previous research studies have only used time domain factors to measure and identify headform and postmortem human subject head impacts (Babbs, 2006; King et al., 2003). A criticism of these studies was that the influence of vibration and frequency of impact acceleration was not considered (Chinn et al., 2001). Many researchers believe rotational acceleration to be important as a factor for head injury

tolerance criteria (Babbs, 2006; Chinn et al., 2001; Gennarelli, 1993; King et al., 2003; Versace, 1993). It was suggested that it may be possible to better identify the rotational acceleration experienced by a headform using linear accelerometer sets if the impact angle, or impact site, was further defined (Crisco et al., 2004; Padgaonkar et al., 1975). It has been further suggested that frequency domain factors could be beneficial in impact severity prediction by helping to complete the headform movement explanation (Chinn et al., 2001). From the current study, it was shown that an improvement in impact site, location, and orientation prediction ratio existed when frequency domain factors were considered.

Several studies have investigated the addition and refinement of measures of head impacts in order to better describe the impact outcome (Babbs, 2006; Gadd, 1993; Goldsmith, 1981; Got et al., 1993; Gurdjian, 1975; Lighthall, 1993; King et al., 2003; Ward, 1993). The results of this study have shown that frequency information inherent in the data signal can be used to improve analyses. The mathematical transforms required to produce the frequency domain variables are readily available.

When comparing each classification subcategory as shown in Table 13 and Table 21, the inclusion of frequency domain factors improved each of the prediction ratios by approximately 3 to 21 percent. There were two exceptions to this improvement. For both the 0.2m drops without considering impact site and 0.4m perpendicular trials, no change was shown with the addition of frequency domain factors as potential determinants. This was due to the omission of the measured fundamental frequency in both cases and measured frequency ratio for 0.2m drops without considering impact site from the canonical discriminant functions. These factor

absences were a result of sub-threshold *F* to enter values for the noted variables during the development of the particular functions. Interestingly, the subcategory of 0.4m perpendicular impacts incorporated headform acceleration as a factor only in the frequency domain exclusion model, but the inclusion and exclusion models were equally efficient as predictors of the subcategory. The 0.4m perpendicular subcategory was also the worst predicted subcategory with only 36.7 percent of the function prediction outcomes being correct.

The results obtained from this study revealed that the inclusion of the frequency domain factors of fundamental frequency and frequency ratio significantly improved the ability of the mathematical model to properly identify each of drop height, headform orientation, and impact site as shown in Table 22. The largest improvement from Table 22 was in predicting impact site with the use of the predicted drop height and headform orientation, which was the stated purpose of the present study.

With respect to the primary purpose of the present study, it was found that the frequency domain inclusion model was able to correctly predict the three desired variables of drop height, headform orientation, and impact site in approximately 54 percent of the primary trials. This percentage was supported through secondary trial analysis using the unstandardized canonical discriminant functions derived from the primary data. The more traditional impact tolerance model excluding frequency domain factors used only force in the vertical axis, headform acceleration, and center of pressure displacement as predictors for the target variables. In the present study, the exclusion model was ten percent less efficient than the inclusion model in predicting with below 44 percent accuracy when attempting to identify all three desired categorical

variables. As shown in Table 23, no significant differences were found when comparing the prediction ratio of the primary data versus secondary data. Data that was not used in creating the unstandardized canonical discriminant functions had the same probability of being correctly identified by the functions. This supported the reliability of the functions when assessing data within the study delimitations of 0.2 and 0.4m drop heights, perpendicular and tangential headform orientations, and the six impact sites. For an unstandardized canonical discriminant model to represent a wider range of headform impacts and eventually to be able to generalize findings to direct and indirect head impacts several further factors must be considered. Additional drops from different drop heights and with more impact sites and headform orientations would permit the current model to be expanded to differentiate among a greater range of headform impact scenarios. For the theoretical leap from headform impact definition to head impact outcome prediction to be possible further factors must be considered. A headform with more biofidelic characteristics as a part of a complete model human anthropometric test device would represent the next evolution of test device that could be used to implement concepts of frequency domain inclusion established in the current study in the testing of a wider variety of head trauma. Such a test device could also expand the range of testing using frequency domain factors to include impact trauma to the neck and potentially limbs and torso impacts.

SUMMARY, CONCLUSION, AND FUTURE RECOMMENDATIONS

Summary

Head injury is the most common severely disabling injury in the United States and is associated with huge financial costs and lifelong disability. Injury prevention is the most efficient method to mitigate the effect of head trauma. In order to prevent head injuries, a better understanding of the causes of head trauma is required. Previous research has focused primarily on linear acceleration of the head as a single factor in injury prediction; however, many researchers have shown that additional impact information is required to properly quantify injurious events. Many biomechanical factors have been investigated with respect to prediction of head injury outcome, including rotational acceleration, internal pressure changes, elastic skull deformation, and individual cranial geometry. This study investigated the potential benefit of applying acceleration frequency domain factors in the analysis of headform impacts with an objective of enhanced comprehension of impact conditions.

A five kilogram headform was dropped a total of 560 times in relative free-fall using a modified Headform Impact Measurement Device from heights of 0.2 and 0.4 meters under twelve drop conditions. The conditions were defined by six impact sites and two headform orientations or impact angles. Voltage measurements were recorded using a triaxial piezoelectric acceleration transducer mounted at the center of mass of the headform, as well as from an AMTI force platform to which the modified Headform Impact Measurement Device was securely fastened. Center of pressure values were calculated based on linear and rotational forces acting on the force platform. A discriminant function model was created using the three factors of linear acceleration,

vertical force, and center of pressure to predict three impacts conditions. The three predicted conditions, drop height, headform orientation, and impact site, were compared to the known drop conditions for each trial.

Two frequency domain factors were established using a fast-Fourier transform. The factors were namely the fundamental frequency, as defined by the spectral value with the greatest power, and the ratio of high to low frequency power, with the median frequency of 250Hz as the demarcation threshold frequency. A second discriminant function model was created using the three previous factors of linear acceleration, vertical force, and center of pressure and the two frequency domain factors to predict three impacts conditions. The three predicted conditions, drop height, headform orientation, and impact site, were again compared to the known drop conditions for each trial.

A comparison of the two discriminant function models established the effective changes associated with including the frequency domain factors in the analysis of headform impacts. After the two models were compared, secondary test data was analyzed using both models to verify prediction ratios for multiple impact scenarios.

Significant prediction outcome improvements were recorded for each of the three drop conditions when the frequency domain factors were included. The headform orientation prediction ratio showed an increase of four percent, which was significant at the $p < 0.05$ level. The prediction ratio increases for both the headform drop height and impact site were significant at the $p < 0.01$ level, with three and ten percent increases, respectively.

The prediction ratios established by the model data did not differ significantly from the ratios determined through the secondary test data for any of the testing scenarios. This comparison is presented in Table 23.

Conclusion

Drop height, headform orientation, and location of an impact were evaluated based on specific time and frequency domain factors recorded in perpendicular and tangential headform impacts. In particular, the extent to which fundamental frequency, high to low frequency ratio, vertical force, headform acceleration and center of pressure measures can be used to identify the height, orientation, and location of a headform impact was investigated. Acknowledging the intrinsic generalization limitations due to the use of a headform as opposed to a live human subject, results indicated that the use of the frequency domain inclusion model was beneficial in analyzing direct perpendicular and tangential impacts when compared to the frequency domain exclusion model. An increase in outcome prediction accuracy of ten percent was recorded through the incorporation of fundamental frequency and high to low frequency ratio factors in unstandardized canonical discriminant functions. This was achieved with data inherent to traditional headform impact testing and could potentially be incorporated into other tolerance algorithms by head impact researchers. The use of frequency domain factors may be of most benefit when predicting angular acceleration based on measured linear acceleration, as it could eliminate large amounts of signal noise without deleting true signal. This would improve measurement efficiency and effectiveness, potentially allowing a better understanding of human head injury tolerance criteria.

Future Recommendations

The following recommendations are proposed for future research:

1. Using the methodology and protocols from this study, additional drop heights, headform orientations, and impact sites could be analyzed to increase the variability and generalization of the findings to extend to more head impact scenarios.
2. The modified Headform Impact Measurement Device could be adapted to incorporate a more biofidelic headform, allowing for a more realistic understanding of the influence of frequency domain inclusion model with respect to head impacts.
3. The modified Headform Impact Measurement Device could be further altered to allow for headform rotation through neck compliance. This would permit rotational acceleration of the headform to be assessed directly.
4. Indirect impacts could be assessed with a frequency domain inclusion model using an alternative method for creating impacts, such as a linear impactor, weighted pendulum, or automotive crash reconstruction, and either postmortem human subjects or a complete model human anthropometric test device. This would further the understanding of the influence of the frequency domain factors in potentially concussive events.
5. Investigations could be conducting regarding the benefit of incorporating frequency domain factors into tolerance criteria such as the Head Injury Criterion or Generalized Acceleration Model for Brain Injury Tolerance in order to more accurately discriminate injury severity.

REFERENCES

ADInstruments Pty Ltd. (2006). *PowerLab 16/30 Series Owners Guide.* Bella Vista, Australia.

Advanced Mechanical Technology, Inc. (1990). *Biomechanics Data-Acquisition and Analysis Software: Operating Manual.* Newton, MA.

Advanced Mechanical Technology, Inc. (1987). *Model OR6-5-1 Biomechanics Platform Instruction Manual.* Newton, MA.

Antonsson, E. K., Mann, R. W. (1985). The frequency content of gait. *Journal of Biomechanics, 18*(1), 39-47.

Babbs, C. F. (2006). A new biomechanical head injury criterion. *Journal of Mechanics in Medicine and Biology, 6*(4), 349-371.

Beer, F. P., & Johnston, J. E. (1976). *Mechanics for engineers: Dynamics* (3rd ed.). Toronto: McGraw-Hill.

Bishop, P. J., Norman, R. W., & Kozey, J. W. (1984). An evaluation of football helmets under impact conditions. *The American Journal of Sports Medicine, 12*(3), 233-236.

Bishop, P. J., & Wells, R. P. (1990). The inappropriateness of helmet drop tests in assessing neck protection in head-first impacts. *The American Journal of Sports Medicine, 18*(2), 201-205.

Brands, D. W., Bovendeerd, P. H., & Wismans, J. S. (2002). On the potential importance of non-linear viscoelastic material modeling for numerical prediction of brain tissue response: Test and application. *Stapp Car Crash Journal, 46*, 1-19.

Cantu, R. C. (2001). Posttraumatic retrograde and anterograde amnesia: Pathophysiology and implications in grading and safe return to play. *Journal of Athletic Training, 26*(3), 244-248.

Cardou, P., & Angeles, J. (2008). Estimating the angular Velocity of a rigid body moving in the plane from tangential and centripetal acceleration measurements. *Multibody System Dynamics, 19*(4), 383-406.

Caswell, S. V., & Deivert, R. G. (2002). Lacrosse helmet designs and the effects of impact forces. *Journal of Athletic Training, 37*(2), 164-171.

Chinn, B., Canaple, B., Derler, S., Doyle, D., Otte, D., Schuller, E., et al. (2001). Cost 327: Motorcycle safety helmets. *Final Report of Action.* (B. Chinn, Ed.) Belgium: Office for Official Publications of the European Communities.

Clancy, E. A, Farina, D., Merletti, R. (2005). Cross-comparison of time- and frequency-domain methods for monitoring the myoelectric signal during a cyclic, force-varying, fatiguing hand-grip task. *Journal of Electromyography and Kinesiology, 15*(3), 256-265.

Crisco, J. J., Chu, J. J., & Greenwald, R. M. (2004). An algorithm for estimating acceleration magnitude and impact location using multiple nonorthogonal single-axis accelerometers. *Journal of Biomechanical Engineering, 126*(6), 849-854.

de Leva, P. (1996). Adjustments to Zatsiorsky-Seluyanov's segment inertia parameters. *Journal of Biomechanics, 29*(9), 1223-1230.

Diekhoff, G. (1992). *Statistics for the social and behavioral sciences: Univariate, bivariate, multivariate.* Dubuque, IA: Wm. C. Brown.

Duma, S. M., Manoogian, S. J., Bussone, W. R., Brolinson, P. G., Goforth, M. W., Donnenwerth, J. J., Greenwald, R. M., Chu, J. J., & Crisco, J.J. (2005). Analysis of real-time head accelerations in collegiate football players. *Clinical Journal of Sports Medicine, 15*(1), 3-8.

Ebenbichler, G. R., Bonato, P., Roy, S. H., Lehr, S., Posch, M., Kollmitzer, J., et al (2002). Reliability of EMG time-frequency measures of fatigue during repetitive lifting. *Medicine and Science in Sports and Exercise, 34*(8), 1316-1323.

Frankowski, R. F., Annegers, J. F., & Whitman, S. (1985). Epidemiological and descriptive studies. Part I: The descriptive eepidemiology of head trauma in the United State. (D. P. Becker, & J. T. Ovlishock, Eds.) *Central Nervous System Trauma Status Report*, 33-44.

Gadd, C. W. (1993). Use of weighted-impulse criterion for estimating injury hazard. In S. H. Backaitis (Ed.), *Biomechanics of Impact Injury and Injury Tolerance of the Head-Neck Complex* (pp. 249-254). Warrendale, PA: Society of Automotive Engineers, Inc.

Gagnon, M., Robertson, G., & Norman, R. (1987). Kinetics. In D. A. Dainty, & R. W. Norman (Eds.), *Standardizing Biomechanical Testing in Sport* (pp. 21-57). Champaign, IL: Human Kinetics.

Gennarelli, T. A., Thibault, L. E., Tomei, G., Wiser, R., Graham, D., & Adams, J. (1993). Directional dependence of axonal brain injury due to centroidal and non-centroidal acceleration. In S. H. Backaitis (Ed.), *Biomechanics of Impact Injury and Injury Tolerance of the Head-Neck Complex* (pp. 595-599). Warrendale, PA: Society of Automotive Engineers, Inc.

Goldsmith, W. (1981). Current controversies in the stipulation of head injury criteria. *Journal of Biomechanics , 14*(12), 883-884.

Got, C., Patel, A., Fayon, A., Tarrière, C., & Walfisch, G. (1993). Results of experimental head impacts on cadavers: The various data obtained and their relations to some measured physical parameters. In S. H. Backaitis (Ed.), *Biomechanics of Impact Injury and Injury Tolerance of the Head-Neck Complex* (pp. 441-483). Warrendale, PA: Society of Automotive Engineers, Inc.

Griffiths, I. W. (2006). *Principles of biomechanics & motion analysis.* Philidelphia, PA: Lippincott Williams & Wilkins.

Gronwall, D. (1991). Minor head injury. *Neuropsychology, 5*(4), 253-265.

Gurdjian, E. S. (1975). *Impact head injury: Mechanistic, clinical and preventive correlations*. Springfield, IL: Charles C Thomas.

Gurdjian, E. S., & Gurdjian, E. S. (1978). Acute head injuries. *Surgery, Gynecology & Obstetrics, 146*, 805-820.

Guskiewicz, K. M., & Mihalik, J. P. (2006). The biomechanics and pathomechanics of sport-related concussion. In S. M. Slobounov, & W. J. Sebastianelli (Eds.), *Foundations of Sport-Related Brain Injuries* (pp. 65-83). Springer, US.

Hamill, J., & Knutsen, K. M. (1995). *Biomechanical basis of human movement.* Philidelphia, PA: Williams & Wilkins.

Hoshizaki, T. B., & Brien, S. E. (2004). The science and design of head protection in sport. *Neurosurgery , 55*(4), 956-967.

King, A., I., Yang, K., H., Zhang, L., Hardy, W., Viano, D., C. (2003, September). Is head injury caused by linear or angular acceleration? *Proceedings of the IRCOBI conference, Portugal.*

Lighthall, J. W., Melvin, J. W., & Ueno, K. (1993). Toward a biomechanical criterion for functional brain injury. In S. H. Backaitis (Ed.), *Biomechanics of Impact Injury and Injury Tolerance of the Head-Neck Complex* (pp. 621-627). Warrendale, PA: Society of Automotive Engineers, Inc.

Lockett, F. J. (1985). Biomechanics justification for empirical head tolerance criteria. *Journal of Biomechanics , 18*(3), 217-224.

Marsh, P. K. (2007). Wizards of motion: Evaluation of a helmet intervention program (Masters Dissertation, Lakehead University). *National Library of Canada: Acquisitions and Bibliographic Services.*

McCrory, P., Johnston, K., Meeuwisse, W., Aubry, M., Cantu, R., Dvorak, J., et al. (2005). Summary and agreement statement of the 2nd international conference on concussion in sport, Prague 2004. *British Journal of Sports Medicine, 39*, 196-204.

Mertz, H., & Patrick, L. (1993). Investigation of the kinematics and kinetics of whiplash. In S. H. Backaitis (Ed.), *Biomechanics of Impact Injury and Injury Tolerance of the Head-Neck Complex* (pp. 43-72). Warrendale, PA: Society of Automotive Engineers, Inc.

Miller, I., & Miller, M. (1999). *John E. Freund's mathematical statistics.* Toronto: Pearson Education.

Moser, R. S., & Schatz, P. (2002). Enduring effects of concussion in youth athletes. *Archives of Clinical Neuropsychology, 17*, 91-100.

National Operating Committee on Standards for Athletic Equipment. (2007). *Standard drop test method and equipment used in evaluating the performance characteristics of protective headgear.*

Newman, J. A., Beusenberg, M. C., Shewchenko, N., Withnall, C., & Fournier, E. (2005). Verification of biomechanical methods employed in a comprehensive study of mild traumatic brain injury and the effectiveness of American football helmets. *Journal of Biomechanics, 38*(7), 1469-1481.

Padgaonkar, A. J., Krieger, K. W., & King, A. I. (1975). Measurement of angular acceleration of a rigid body using linear accelerometers. *Journal of Applied Mechanics, 42* (3), 552-556.

Pellman, E. J., Viano, D. C., Tucker, A. M., & Casson, I. R. (2003). Concussion in professional football: Location and direction of helmet impacts - Part 2. *Neurosurgery, 53*(6), 1328-1341.

Pellman, E. J., Viano, D. C., Tucker, A. M., Casson, I. R., & Waeckerle, J. F. (2003). Concussion in professional football: Reconstruction of game impacts and Injuries. *Neurosurgery, 53*(4), 799-814.

Sances Jr, A., Larson, S. J., Yoganandan, N., & Pintar, F. A. (Eds.). (2000). Frontiers in head and neck trauma: Clinical and biomechanical. I O S Press, Incorporated.

Sarkar, S., Majumder, S., & Roychowdhury, A. (2004). Response of human head under static & dynamic load using finite element method. *Trends in Biomaterials & Artificial Organs, 17*(2), 130-134.

Schulz, M. R., Marshall, S. W., Mueller, F. O., Yang, J., Weaver, N. L., Kalsbeek, W. D., et al. (2004). Incidence and risk factors for concussion in high school athletes, North Carolina, 1996-1999. *American Journal of Epidemiology, 160*(10), 937-944.

Smith, S. W. (2002). Discrete fourier transform. In *The Scientist and Engineer's Guide to Digital Signal Processing* (pp. 141-168). California Technical Publishing.

Spyrou, E. (1997). The effects of shell geometry on the impact attenuation capabilities and impact conditions (Masters Dissertation, McGill University). *National Library of Canada: Acquisitions and Bibliographic Services.*

Spyrou, E., Pearsall, D. J., & Hoshizaki, T. B. (2000). Effect of local shell geometry and material properties on impact attenuation of ice hockey helmets. *Sports Engineering, 3*, 23-35.

Suits, B. H. (2006). *Frequencies for equal-tempered scale.* (Physics Department, Michigan Technological University) Retrieved December 6, 2007, from Physics of Music - Notes: http://www.phy.mtu.edu/~suits/notefreqs.html

Tortora, G. J. (2002). An introduction to the human body. In *Principles of Human Anatomy* (pp. 1-24). Hoboken, NJ: John Wiley & Sons, Inc.

United States Department of Health and Human Services. (1989). Healthy people 2000 - national health promotion and disease prevention objectives. 692.

Versace, J. (1993). A review of the severity index. In S. H. Backaitis (Ed.), *Biomechanics of Impact Injury and Injury Tolerance of the Head-Neck Complex* (pp. 309-334). Warrendale, PA: Society of Automotive Engineers, Inc.

Voo, L., Kumaresan, S., Pintar, F. A., Yoganandan, N., & Sances, A. (1996). Finite-element models of the human head. *Medical & Biological Engineering & Computing, 34*, 375-381.

Ward, C., Chan, M., & Nahum, A. (1993). Intracranial pressure: A brain injury criterion. In S. H. Backaitis (Ed.), *Biomechanics of Impact Injury and Injury Tolerance of the Head-Neck Complex* (pp. 347-360). Warrendale, PA: Society of Automotive Engineers, Inc.

White, R., Agouris, I., & Fletcher, E. (2005). Harmonic analysis of force platform data in normal and cerebral palsy gait. *Clinical Biomechanics, 20*(5), 508-516.

Whitnall, C., Shewchenko, N., Gittens, R., & Dvorak, J. (2005). Biomechanical investigation of head impact in football. *British Journal of Sports Medicine, 39* (Suppl I), i49-i57.

Whitnall, C., Shewchenko, N., Wonnacott, M., & Dvorak, J. (2005). Effectiveness of headgear in football. *British Journal of Sports Medicine, 39*(Suppl I), i40-i48.

Yoganandan, N., Pintar, F. A., Zhang, J., Stemper, B. D., & Philippens, M. (2008). Upper neck forces and moments and cranial angular accelerations in lateral impact. *Annals of Biomedical Engineering, 36*(3), 406-414.

Yoganandan, N., Zhang, J., Pintar, F. A., & Liu, Y. K. (2006). Lightweight low-profile nine-accelerometer package to obtain head angular accelerations in short-duration impacts. *Journal of Biomechanics, 39*(7), 1347-1354.

APPENDIX A

Operational Definitions

Azimuth → The measured angle along the basic plane with zero defined as the posterior intersection of the basic and mid-sagittal planes and counterclockwise rotation as positive. The symbol for azimuth is θ and locations on the head may be defined as having some angle in the azimuth and some elevation (e.g. Top Boss$\left[\theta = \pi, \phi = \frac{\pi}{4}\right]$) (Crisco, Chu, & Greenwald, 2004).

Basic Plane → A transverse anatomical plane that includes the cranial edge of the external auditory meatuses and the caudal notches of the orbital ridges. The basic plane is also referred to as the Frankfort plane (National Operating Committee on Standards for Athletic Equipment, 2007).

Coronal Plane → A vertical plane that passes through the midline of the body, which divides the body into equal anterior and posterior halves. The coronal plane is orthogonally aligned to the mid-sagittal and reference transverse planes (Tortora, 2002).

Drop Height → The vertical distance measured from the strike plate of the Headform Impact Measurement Device to the base of the headform at release. For this study, distances of 0.2, 0.4, and 0.6 meters are being implemented.

Durometer → A scale of measurement indicating a material's resistance to permanent indentation. The depth of indentation of a 6.4mm thick material sample is graded from 100, no indentation, to 0, greater than or equal to 2.5mm of indentation. To create an indentation, type D testing uses a hardened steel rod of diameter 1.1-1.4mm, with a 30° conical point and 0.1mm tip radius, applied with 44.64N of steady force.

Elevation → The measured angle superior to the basic plane with zero defined as being along the basic plane and $\frac{\pi}{2}$ being at the Top location. The symbol for elevation is ϕ and locations on the head may be defined as having some angle in the azimuth and some elevation (e.g. Top Boss$\left[\theta = \pi, \phi = \frac{\pi}{4}\right]$) (Crisco, Chu, & Greenwald, 2004).

Front → An impact location marked at the point 0.0254m cranially from the anterior intersection of the mid-sagittal plane and the reference transverse plane (NOCSAE, 2007). It is also referred to as Front$[\theta = \pi, \phi = 0]$.

Front Boss → An impact location in the same transverse plane as the Front location, but rotated $\frac{\pi}{4}$ radians (45°) clockwise (NOCSAE, 2007). It is also referred to as Front Boss$\left[\theta = \frac{3\pi}{4}, \phi = 0\right]$.

Headform Impact Measurement Device → An instrumented mechanical device that uses the pull of gravity to accelerate a biofidelic headform along a low-friction rail onto a strike plate in order to simulate head impact trauma.

Headform → A model human head, instrumented with a triaxial piezoelectric accelerometer, designed to fit the Headform Impact Measurement Device assembly, which possess a high biofidelity (NOCSAE, 2007).

Hybrid III → A complete model human anthropometric test device based on cadaveric data, the Hybrid III has sensors throughout its biofidelic body to measure impact forces. The 50th percentile adult Hybrid III dummy is 1.68m tall and weighs 77kg. The Hybrid III is the standard endorsed by the Society of Automotive Engineers.

Mid-Sagittal Plane → A vertical plane that passes through the midline of the body, which divides the body into equal left and right halves. The midsagittal plane is orthogonally aligned to the coronal and reference transverse planes (Tortora, 2002).

Rear → An impact location marked at the posterior intersection of the midsagittal plane and the reference transverse plane (NOCSAE, 2007). It is also referred to as Rear$[\theta = 0, \phi = 0]$.

Rear Boss→ An impact location that is rotated $\frac{\pi}{4}$ radians (45°) counterclockwise along the reference transverse plane from the rear impact location (NOCSAE, 2007). It is also referred to as Rear Boss$\left[\theta = \frac{\pi}{4}, \phi = 0\right]$.

Reference Transverse Plane → A transverse anatomical plane that runs parallel, at a distance of 0.06m cranially, to the basic plane (NOCSAE, 2007).

Side → An impact location marked at the point 0.0254m cranially from the intersection of the coronal plane and the reference transverse plane (NOCSAE, 2007). It is also referred to as Side$\left[\theta = \frac{\pi}{2}, \phi = 0\right]$.

Top Boss → An impact location defined in this testing as a point that is rotated $\frac{\pi}{4}$ radians (45°) anterior to the top impact site along the mig-sagittal plane. It is also referred to as Top Boss$\left[\theta = \pi, \phi = \frac{\pi}{4}\right]$.

Physics Terminology

Acceleration → The rate of change of linear velocity expressed in meters per second squared $(\frac{m}{s^2})$, as denoted by $\vec{a}$. In impact biomechanics, accelerations are often discussed in terms multiples of gravity, $\vec{g}$ (Hamill & Knutsen, 1995).

Angular Acceleration → The rate of change of angular velocity expressed in radians per second squared ($\frac{rad}{s^2}$), denoted as $\vec{\alpha}$. It may also be understood as the derivative of angular velocity and represents the slope of either a secant, being the average value, or a tangent, being an instantaneous value (Hamill & Knutsen, 1995).

Fast Fourier Transformation → A mathematical method, involving the splitting of real and complex numbers, used to convert a waveform from a function expressed in terms of time to a function expressed in terms of component frequencies (Smith, 2002).

Force → Any vector interaction between two objects that can cause an object to accelerate either positively or negatively. It is expressed as being directly proportional to both the mass and acceleration of an object and is denoted as $\vec{F}$ (Hamill & Knutsen, 1995).

$\overrightarrow{F_x}$ → The force in the mediolateral axis (Advanced Mechanical Technology, Inc, 1990).

$\overrightarrow{F_y}$ → The force in the anteroposterior axis (AMTI, 1990).

$\overrightarrow{F_z}$ → The force in the vertical axis (AMTI, 1990).

Frequency → A measure of how often cycles of a waveform occur within a defined period of time, usually one second. It is displayed in Hertz (Hz), which represent the repetition rate per second or the inverse of a cycle's period (Smith, 2002).

$\vec{g}$ → A unit of acceleration equal to the acceleration due to gravity or approximately 9.81 $\frac{m}{s^2}$ directed downward (Griffiths, 2006).

Harmonic → If a signal is periodic with frequency f, the only frequencies composing the signal are integer multiples of f, i.e. f, $2f$, $3f$, etc. These frequencies are called harmonics. The first harmonic is f, the second harmonic is $2f$, the third

harmonic is $3f$, and so forth. The first harmonic is also given a special name, the fundamental frequency (Smith, 2002).

Mass → A constant measure of the amount of matter that constitutes an object and is expressed in kilograms (kg) (Hamill & Knutsen, 1995).

Moment of Force or Torque → A vector quantity consisting of the product of force and the perpendicular distance from the axis of rotation to the line of action of the force. It is expressed in Newton-meters (N · m) and is the rotational equivalent of force (Gagnon, Robertson, & Norman, 1987).

$\overrightarrow{M_x}$ → The moment about the mediolateral axis (AMTI, 1990).

$\overrightarrow{M_y}$ → The moment about the anteroposterior axis (AMTI, 1990).

$\overrightarrow{M_z}$ → The moment about the vertical axis (AMTI, 1990).

APPENDIX B

Pilot Investigation

Purpose

An initial pilot study was conducted to determine estimates of reliability and validity for the modified Headform Impact Measurement Device. The pilot study addressed the following three objectives:

Objectives

To investigate the relationship between vertical acceleration measures from the modified Headform Impact Measurement Device and the vertical force measures from the Advanced Mechanical Technologies, Inc force platform.

To determine the inter-reliability of measurement response, with respect to vertical acceleration magnitude and frequency, for the modified Headform Impact Measurement Device.

To determine the intra-reliability of measurement response, with respect to vertical acceleration magnitude and frequency, for the modified Headform Impact Measurement Device.

To determine the statistical power based on drop quantity, specifically comparing the use of twenty trials to one hundred trials.

Instruments

Modified Headform Impact Measurement Device

The original Headform Impact Measurement Device was based on the Canadian Standards Association (CSA) helmet testing equipment. The device, shown in Figure 3, measured eighty centimetre (0.80m) and was constructed at Lakehead University

through collaboration between the faculties of Kinesiology and Engineering (Marsh, 2007). A triaxial accelerometer was placed at the center of mass of a five kilogram (5kg) headform with a sensitive axis aligned to within five degrees (5°) of vertical. The triaxial accelerometer used a small piezoelectric acceleration transducer with three orthogonal axes. It was designed to measure vibration in three mutually exclusive axes. The headform was connected to a vertical low-friction rail, extending from the top of the device inferiorly to a point seventeen centimetres (0.17m) above the bottom plate, to allow for standardized drops.

The cast urethane headform was designed to approximate the mass and size of an adult human head at 5 kilograms and 0.61 meters in circumference about the reference plane. The headform had a neck with zero compliance so that the path of the head while falling was linear. After release, the headform fell along the vertical low-friction rail solely as a result of gravity.

The headform struck a polytetrafluoroethylene (PTFE) plate measuring 0.10 meters in diameter and 0.023 meters in height, with a tensile strength of 26.89 MPa and a durometer reading of D50 on the shore hardness scale. This hardness value approximated the impact that would be sustained against a hockey helmet. The strike plate then mechanically transferred the impact through a 0.010 meter aluminium disk into an AMTI force platform.

The vertical mono-rail track on the original Headform Impact Measurement Device was extended inferiorly to the bottom plate to guard against the headform derailing under dynamic impact conditions. The strike plate at the center of the bottom plate was reduced in height and reinforced to reduce unwanted vibrations within the

device. The Modified Headform Impact Measurement Device was securely fastened to an AMTI force platform in a manner that minimized vibration between the two measurement tools.

AMTI Force Platform

An AMTI force platform fitted with four load cells (exterior dimensions 0.508, 0.464, and 0.0826m, respectively) was used to quantify forces and moments being applied to its surface. Foil strain gages are attached to each of the load cells to form six Wheatstone bridges, with three of the output voltages indicating the proportional level of force in the three axes and the remaining three indicating the measured amount of moment about each of the axes. The force platform was designed to be firmly mounted to a rigid surface for optimal linearity and minimal crosstalk.

Upper limits for platform loading were calculated based on a formula (Equation 10 in Appendix C), which accounted for force in each of the axes, the moment about the vertical axis, and the location of the load on the surface of the platform (Advanced Mechanical Technology, Inc, 1987). The maximumload experienced by the force platform during the testing was well within the prescribed upper limits for the device.

Glockenspiel

A wooden based Sonor Percussion Glockenspiel with metal keys, capable of producing frequencies ranging from 261.5Hz to 698.5Hz, was used in the final task of the pilot investigation. The glockenspiel was firmly fixed with tape to the AMTI force platform during the testing procedures.

Analog-to-Digital Converter

A PowerLab analog-to-digital converter manufactured by ADInstruments was selected for the testing procedures. The converter was capable of handling 400 000 samples per second over eight analog input channels. The converter received analog voltage inputs and transformed the signal into a digital output. The converter then transferred the digitized signal to a computer at up to 840 megabits per second through a USB 2.0 cable. The stated accuracy of the PowerLab analogue-to-digital converter was better than 0.1%; with both zero and gain drift compensation integrated within the unit (ADInstruments Pty Ltd., 2006).

Experimental Tasks

The procedures for the pilot investigation were designed to address each of the four pilot study objectives. The Headform Impact Measurement Device was tested for validity and reliability under multiple scenarios in order to fine-tune the machine and testing protocol. The unhelmeted headform was dropped from various heights under a variety of conditions.

The modified Headform Impact Measurement Device was securely bolted to an AMTI force platform with the top of the head aligned with the positive axis for $\overrightarrow{F_y}$ and the negative axis for $\overrightarrow{F_x}$ on the platform. The headform was oriented for a front impact site and the strike plate was placed in the primary location. Five tasks were completed in the testing of the force platform and the modified Headform Impact Measurement Device.

Task 1: Release technique

For the first testing task, the headform was dropped 200 times from a height of forty centimeters (0.40m). Half of the trials were completed with the headform being

released from the mechanical switch secured at the drop height. The other half of the drops were completed without the use of the mechanical switch, as the headform was held by the examiner prior to release. Vertical linear force voltage values recorded from the force platform were compared between the two groups. It was hypothesized that there would be no significant difference in maximal force values recorded between drops made with and without the mechanical switch.

The set of trials released from the mechanical switch were not significantly different from those dropped without the switch as demonstrated by a *t*-score of $t(199) = 0.6409$, $p > 0.05$ (two-tailed). This supported the hypothesis for Task 1 and indicated that both release mechanisms were considered equal. The impacts in the group released from the mechanical switch were found to have less variability than the manually released trials, with values of 0.7451 and 0.8544 for the standard deviations, respectively, supporting the notion that the mechanical switch was beneficial to the reliability of the testing protocol.

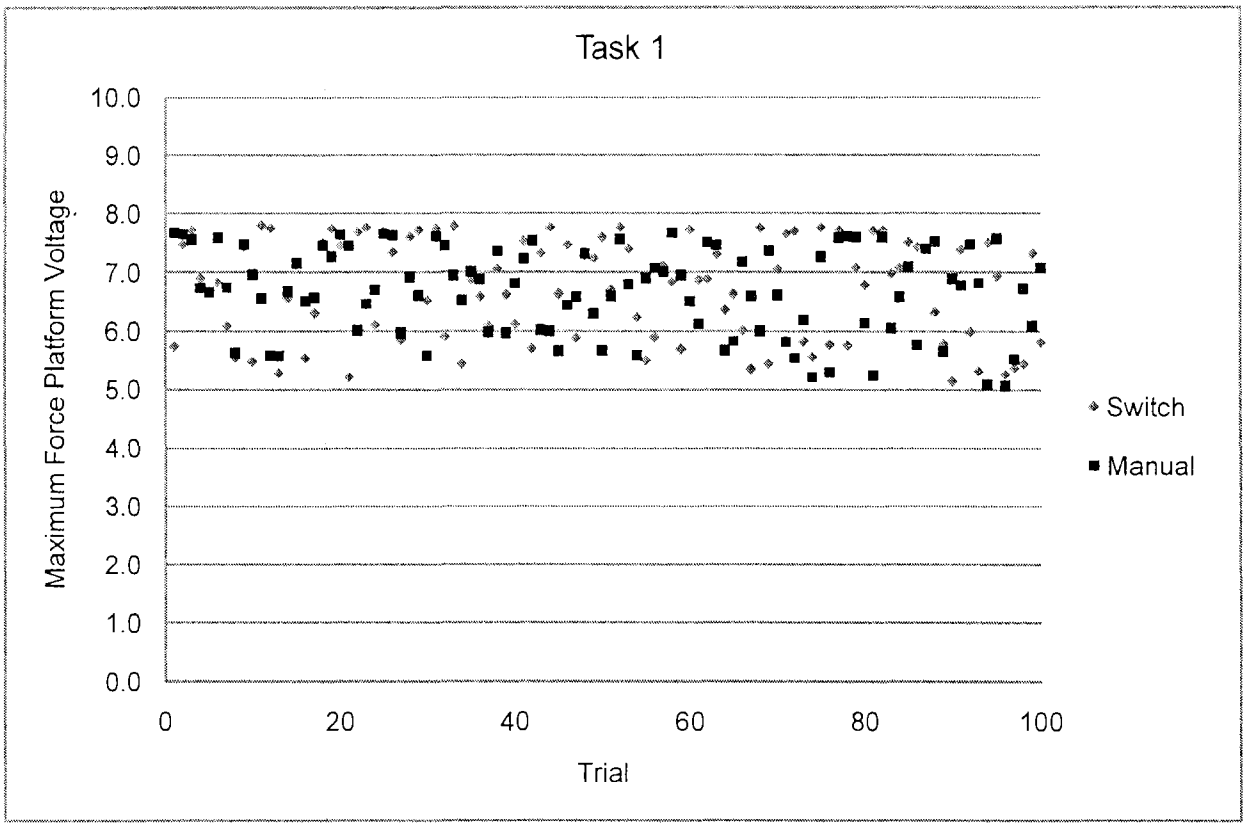

Figure B1. Manual versus Switch Release Technique

Task 2: Strike plate

The data for the 100 trials of the mechanical switch release drops were next used to evaluate the strike plate. In this next comparison, a further 100 trials used the mechanical release and a drop height of forty centimeters, but the PTFE strike plate was removed. Vertical force values recorded for the strike plate impacts were compared to the values recorded when the headform struck the bare metal platform of the Headform Impact Measurement Device. It was hypothesized that there would be no significant difference in maximal force values recorded between drops made with and without the protective PTFE strike plate.

As the testing continued with Task 2, the results showed that there was no significant difference in vertical force voltage values between the two groups. An independent samples *t*-test for groups with unequal variance returned a value of

$t(199) = 0.3967$, $p > 0.05$ (two-tailed). The reliability was actually higher with the PTFE strike plate versus no protective plate. The standard deviation values were 0.7451 and 0.9231, respectively. Therefore, since the *t*-score was not significant and the reliability was greater with the strike plate, the hypothesis for Task 2 was accepted and the Headform Impact Measurement Device was fitted with the protective PTFE strike plate for all subsequent test conditions.

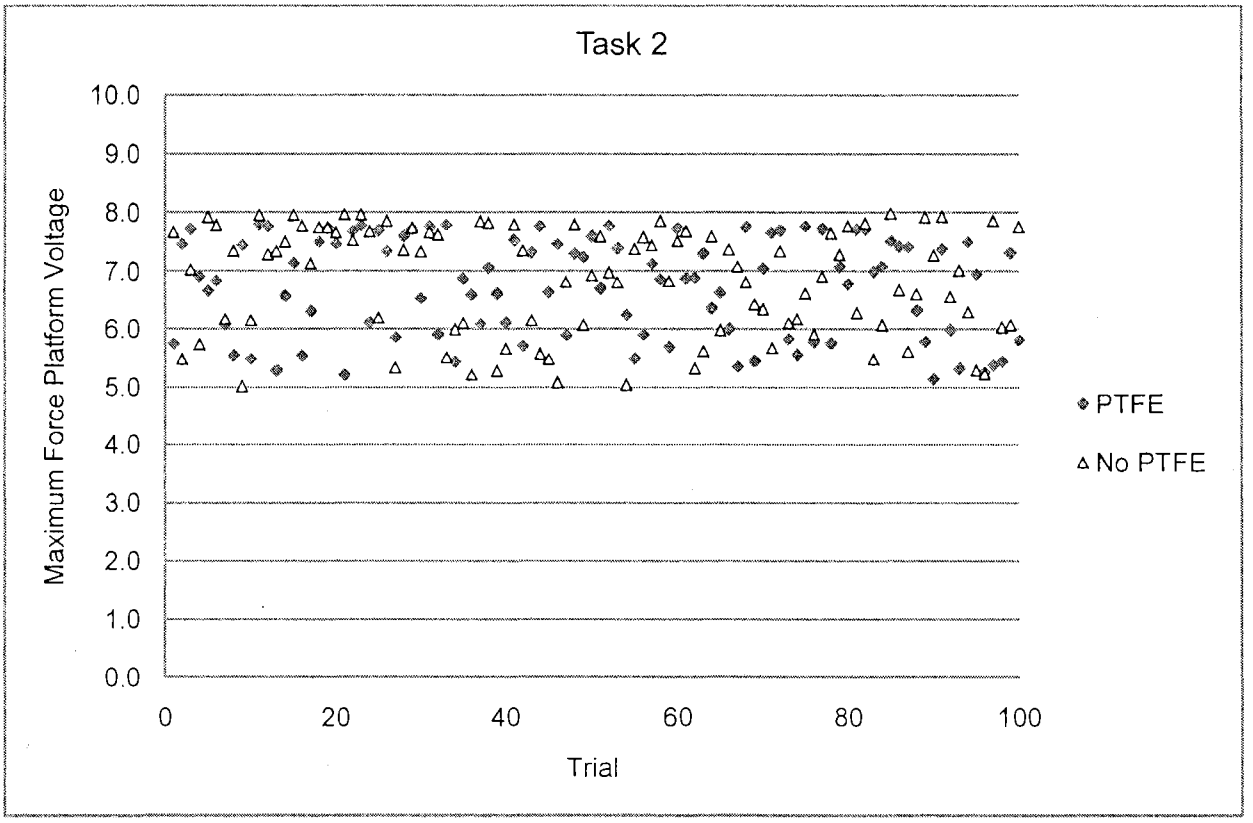

Figure B2. PTFE versus No PTFE Strike Plate

Task 3: Measurement device comparison

Internal consistency was used to test reliability. The concurrent validity of the triaxial accelerometer as compared to the standard of the force platform was assessed by dropping the unhelmeted headform three times each from forty distinct drop heights. Drop heights were increased incrementally by two centimeters (0.02m) ranging from two

centimeters to eighty centimeters (0.02- 0.80m) and each distinct drop height was referred to as a trial block.

The one hundred and twenty trials from the incremental heights in Task 3 were divided into two groups based on trial block. Odd numbered trial blocks made up the first group and even trial blocks defined the second group. The level of correlation between the two groups was determined to be 0.909, or a strong correlation, which preliminarily established the reliability of the data. In addition to the correlation, cronbach's alpha was calculated as 0.879, which was above the threshold value of 0.700 for the coefficient of reliability. This result confirmed the consistency of the data. Further, a repeated measures *t*-test for related samples was calculated using the mean values from each of the trial blocks. The *t*-score was 0.829, which was not significant at the $p < 0.05$ level. The level of intra-reliability between the vertical acceleration measures from the modified Headform Impact Measurement Device and vertical force measures from the AMTI force platform was proven to be acceptable through each of the three analyses of the testing procedures. This indicated that both measurement devices were recording the same outcome from the events and supported the use of both tools.

A noticeable drop in voltage values at the higher drop heights may indicate a saturation of the measurement device. Therefore, a maximum useable drop height of 0.60m could be used for testing procedures.

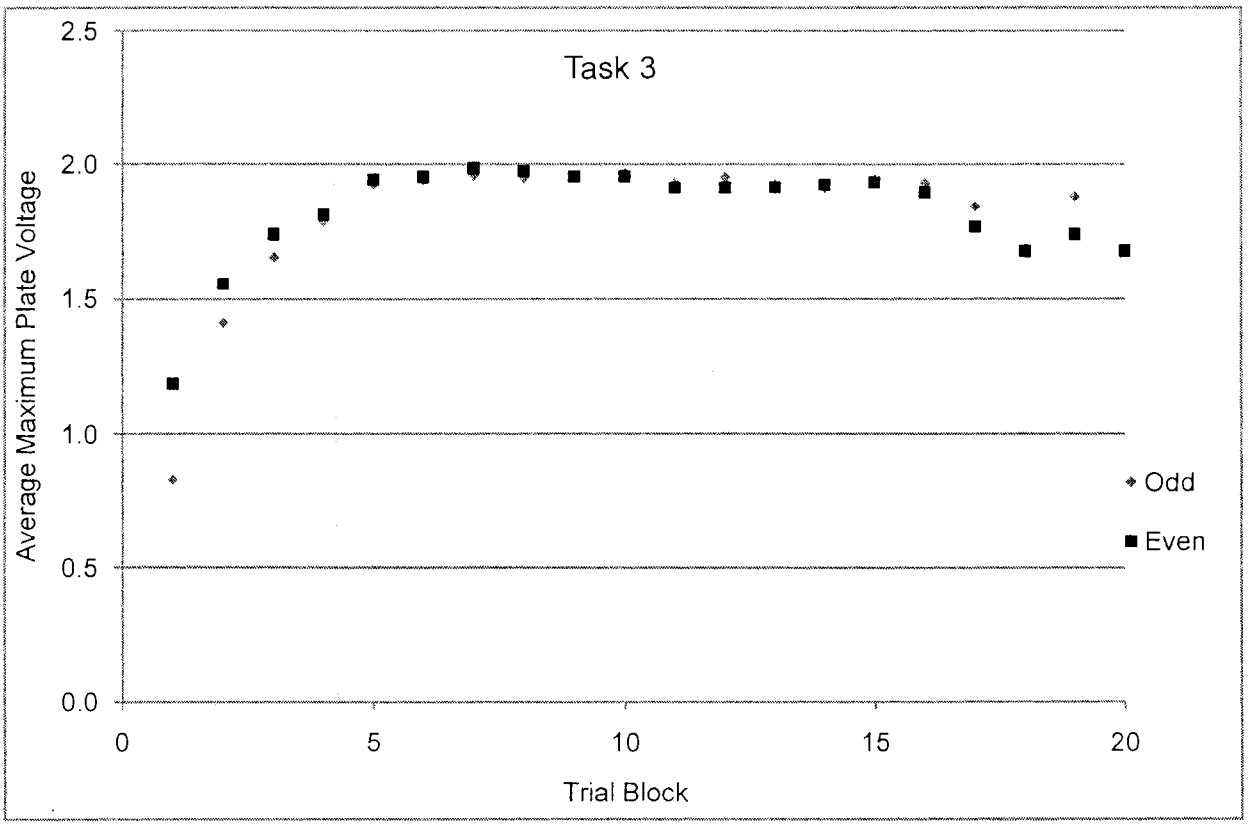

Figure B3. Incremental Drop Height Voltages

Task 4: Drop quantity requirement

Excessive mechanical degradation of the modified Headform Impact Measurement Device would result in unreliable impact measures. Limiting the quantity of drops performed was used as a means of minimizing mechanical wear to the modified Headform Impact Measurement Device. The number of drops to be tested must show the same sampling characteristics as the larger test group of 100 trials. To determine an acceptable sample size, a statistical comparison was used for each measured variable with five levels representing 20, 40, 60, 80, and 100 drops,

respectively. Before a comparison could be made, a Levene's test was administered to ensure homogeneity of variance throughout the independent variable's five levels. As is shown below in Table B1, each of the measured variables other than fundamental frequency did not show significant differences in variance and could be tested using the one-way analysis of variance. The fundamental frequency showed a significant difference and was analyzed using the non-parametric Kruskal-Wallis test.

Table B1

Levene's Test for Homogeneity of Variance

Variable	Levene Statistic	Significance
Vertical Force	0.575	0.681
Headform Acceleration	0.476	0.754
Center of Pressure Displacement	0.584	0.675
Fundamental Frequency	4.299	0.002*
Frequency Ratio	0.197	0.940

*$p < 0.01$. $df = 4$.

As shown in Table B2 and Table B3, no significant differences were found between sample size levels for any of the measured variables.

Table B2

Sample Size One-Way Analysis of Variance

Variable	*F*	Significance
Vertical Force	0.407	0.804
Headform Acceleration	0.078	0.989
Center of Pressure Displacement	0.311	0.871

Frequency Ratio	1.153	0.332

Table B3

Sample Size Kruskal-Wallis Test

Variable	χ^2	Significance
Fundamental Frequency	8.037	0.090

A Tukey's post hoc test was administered for the variables meeting the assumption of homogeneity of variance to ensure no subsample differences existed. For fundamental frequency, a similar non-parametric test was run to identify differences between individual levels. Table B4 and Table B5 below; indicate that no such differences were present. This supported the use of 20 drop samples to minimize the expectantly minimal mechanical changes and assured reliable results throughout the testing procedures.

Table B4

Tukey Post Hoc

Variable	Sample Size	Significance
Vertical Force	20	0.997
	40	0.781
	60	0.998
	80	1.000
Headform Acceleration	20	1.000
	40	0.994
	60	1.000
	80	1.000
Center of Pressure Displacement	20	1.000
	40	0.853
	60	1.000
	80	1.000
Frequency Ratio	20	0.736
	40	0.480
	60	0.966
	80	1.000

Table B5

Non-Parametric Walsh Median Test

Fundamental Frequency	Sample Size				
	20	40	60	80	100
Above Median	8	17	28	34	49
Equal to of Below Median	12	23	32	46	51

Task 5: Glockenspiel frequency recognition

The frequency spectrum values for the force platform were validated by striking a Sonor Percussion Glockenspiel to produce thirteen different frequencies ranging from 261.5Hz to 698.5Hz. The modified Headform Impact Measurement Device was removed from the AMTI force platform and the glockenspiel was fixed to the center of the platform surface. Each musical note was struck in independent trials, followed by trials with multiple notes being struck in quick succession.

The frequency spectrum from the force platform properly identified each independent frequency as it was matched to a corresponding musical note (Suits, 2006). This finding supported the validity of the force platform in the measurement of the frequency spectrum of headform impacts.

Pilot Investigation Discussion

Aspects of the Headform Impact Measurement Device were tested for reliability, namely the release technique and strike plate material. It was found that the method of release influenced the consistency of response and a mechanical release with adjust release height was constructed to allow for more accurate measures. Additionally, it was found that using a protective PTFE strike plate did not influence impact results

significantly and therefore the protective plate will be incorporated in future experiments in order to reduce mechanical wear to the device. After the changes were made to the Headform Impact Measurement Device, with respect to the pilot investigation, the instrument is referred to as the Modified Headform Impact Measurement Device.

The modified Headform Impact Measurement Device and AMTI force platform were found to be consistent and reliable when measuring vertical acceleration and force magnitudes, respectively, under a wide range of drop heights. From the pilot investigation it was determined that testing procedures are reliable with a sample size of 20, but should be kept within a maximum drop height of 60 centimeters to ensure validity. Finally, the AMTI force platform was found to be accurate in identifying the frequency spectrum of musical tones produced with a glockenspiel and was an appropriate tool in measuring impact acceleration frequency.

APPENDIX C

AMTI Force Platform Load Limit

$$\sqrt{7.28\left(\overrightarrow{F_x}^2 + \overrightarrow{F_y}^2\right) + 338\overrightarrow{M_z}^2} + \overrightarrow{F_z}[1 + 5.51(\vec{x} + \vec{y})] \leq 36\,000 \qquad (10)$$

Where $\overrightarrow{F_x}$, $\overrightarrow{F_y}$, and $\overrightarrow{F_z}$ are the forces in Newtons for each of the respective axes;

$\overrightarrow{M_z}$ is the moment or torque in Newton-meters about the vertical axis;

$\vec{x}$ and $\vec{y}$, measured in meters, define the surface location of the load;

And 36 000 is the critical value that may not be exceeded for accurate use.

(AMTI, 1987)

Calculation of Load

Maximum values were taken from each headform impact scenario and a calculation of load was established based on the maximum values. The following calculation demonstration for the perpendicular headform orientation, rear impact site, and 0.4m drop height was the highest scoring of all the groups.

$$Load_{max} = \sqrt{7.28(6.6572\mathrm{V}^2 + 7.1994\mathrm{V}^2) + 338(6.5591\mathrm{V})^2}$$

$$+7.3147\mathrm{V}[1 + 5.51(0.246\mathrm{m} + 0.246\mathrm{m})]$$

$$Load_{max} = 150.6001 \leq 36\,000$$

Since the calculated maximum load was below the threshold value of 36 000, the force platform did not saturate during the impact testing.

APPENDIX D

Setup Procedures and System Specifications

1. Attach the force platform to a cement slab.

Table D1

Platform Dimension Specifications

Height	Width	Depth
0.0826m	0.5080m	0.4640m

Table D2

Platform Bolt Locations

Bolt	Horizontal	Vertical
1	0.1020m	0.0130m
2	0.4070m	0.0130
3	0.1020m	0.4510m
4	0.4070m	0.4510m

2. Set the location of the polytetrafluoroethylene (PTFE) strike plate on the Headform Impact Measurement Device and attach the strike plate with a bolt.

Table D3

Strike Plate Bolt Specifications

	Shaft	Head
Diameter	1.3×10^{-2}m	2.3×10^{-2}m
Depth	2.8×10^{-2}m	8.0×10^{-3}m

3. Attach the Modified Headform Impact Measurement Device to the force platform.

Table D4

Modified Headform Impact Measurement Device Bolt Specifications

	Shaft	Head
Diameter	9.0×10^{-3}m	1.8×10^{-2}m
Depth	3.7×10^{-2}m	7.0×10^{-3}m

Table D5

Modified Head Impact Device Bolt Locations

Bolt	Horizontal	Vertical
1	0.2540m	0.1560m
2	0.3070m	0.1780m
3	0.1990m	0.1780m
4	0.3300m	0.2320m
5	0.1770m	0.2320m
6	0.3070m	0.2850m
7	0.1990m	0.2850m
8	0.2540m	0.3080m

4. Set the filter and gain settings on the amplifiers.

Table D6

AMTI Force Platform Amplifier Settings

Channel	Bridge	Filter	S1	S2	Gain	S3	S4
F_x	5	1 050Hz	Closed	Closed	4 000	Open	Open
F_y	5	1 050Hz	Closed	Closed	4 000	Open	Open
F_z	5	1 050Hz	Closed	Closed	1 000	Closed	Closed
M_x	5	1 050Hz	Closed	Closed	4 000	Open	Open
M_y	5	1 050Hz	Closed	Closed	4 000	Open	Open
M_z	5	1 050Hz	Closed	Closed	4 000	Open	Open

5. Assemble the trigger circuit as per Figure 5.
6. Connect the electronics:
    - AMTI Force platform to AMTI amplifier
    - Accelerometer to unity gain amplifier
    - AMTI amplifier to PowerLab analog-to-digital converter
    - Unity gain amplifier to PowerLab analog-to-digital converter
    - Trigger to PowerLab
    - PowerLab to computer
    - PowerLab, amplifiers, and computer to AC power
    - Trigger to DC power
7. Power ON and initiate software.
8. Chart5 Setup
    - Sampling rate of 1 000Hz

Table D7

Chart5 Channel Definitions

Number	Measure	Label
1	Force along x-axis	F_x
2	Force along y-axis	F_y
3	Vertical Force	F_z
4	Moment about x-axis	M_x
5	Moment about y-axis	M_y
6	Moment about z-axis	M_z
7	Headform acceleration	Headform
8	3V threshold trigger[a]	Trigger

[a] A voltage value of three or greater in channel 8 initiated a four second capture for all of the channels.

9. Set the headform alignment using the reference planes and a protractor.
10. Set the height of the release point with the mechanical switch according to Table 2 or Table 3, respectively.
11. Perform 20 drops:

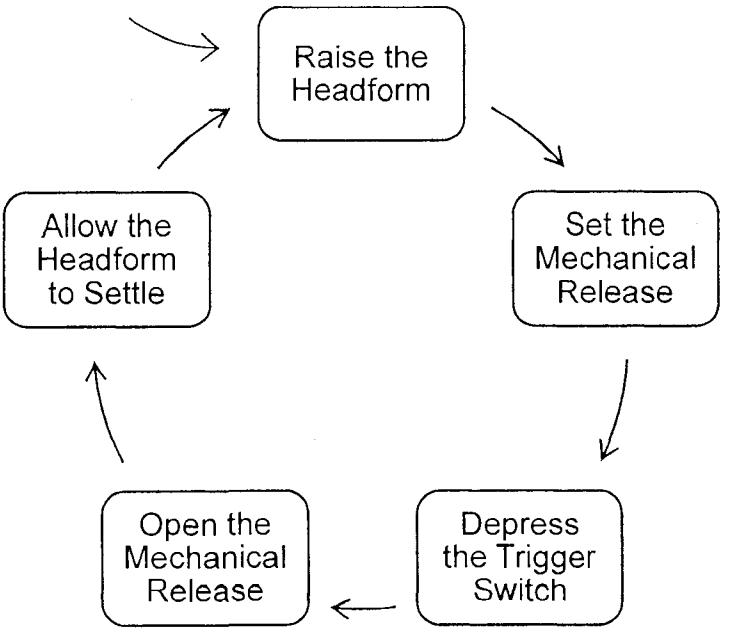

Figure D1. Repeated Individual Drop Procedure

APPENDIX E

Headform Impact Energies and Velocities

Headform Impact Energies

Potential energy of the headform before release was calculated using:

$$\overrightarrow{E_P} = m \times \vec{g} \times \vec{h} \tag{11}$$

Where $\overrightarrow{E_P}$ is the potential energy of the headform prior to release;

m is the mass of the headform;

$\vec{g}$ is the acceleration due to gravity acting on the headform;

and $\vec{h}$ is the drop height. (Hamill & Knutsen, 1995)

Kinetic energy of the headform at the instant of contact with the strike plate was defined by:

$$\overrightarrow{E_K} = \frac{m \times \vec{v}^2}{2} \tag{12}$$

Where $\overrightarrow{E_K}$ is the kinetic energy of the headform at the instant of contact;

m is the mass of the headform;

and $\vec{v}$ is instantaneous velocity of the headform. (Hamill & Knutsen, 1995)

From the conservation of energy, it was known that:

$$\vec{E} = \overrightarrow{E_P} + \overrightarrow{E_K} \tag{13}$$

Where $\vec{E}$ is the total energy of the system;

$\overrightarrow{E_P}$ is the instantaneous potential energy of the headform;

and $\overrightarrow{E_K}$ is the instantaneous kinetic energy of the headform;

(Hamill & Knutsen, 1995)

And since $\overrightarrow{E_K} = 0$ before the headform was released:

$$\vec{E} = m \times \vec{g} \times \vec{h} + 0J \tag{14}$$

Where $\vec{E}$ is the total energy of the system;

m is the mass of the headform;

$\vec{g}$ is the acceleration due to gravity acting on the headform;

and $\vec{h}$ is the drop height. (Hamill & Knutsen, 1995)

Therefore, substituting for both drop heights:

$$\vec{E}_1 = 5kg \times 9.8\frac{m}{s^2} \times 0.2m + 0J \tag{15}$$

$$\vec{E}_1 = 9.8J$$

Where $\vec{E}_1$ is the impact energy for the 0.2m drop height.

$$\vec{E}_2 = 5kg \times 9.8\frac{m}{s^2} \times 0.4m + 0J \tag{16}$$

$$\vec{E}_2 = 19.6J$$

Where $\vec{E}_2$ is the impact energy for the 0.4m drop height.

Impact Velocities

Simplifying for velocity:

$$m \times \vec{g} \times \vec{h} = \frac{m \times \vec{v}^2}{2} \tag{17}$$

$$\vec{g} \times \vec{h} = \frac{\vec{v}^2}{2}$$

$$2 \times \vec{g} \times \vec{h} = \vec{v}^2$$

$$\vec{v} = \sqrt{2 \times \vec{g} \times \vec{h}}$$

$$\vec{v} = \sqrt{19.6 \frac{m}{s^2} \times \vec{h}}$$

Where m is the mass of the headform;

$\vec{g}$ is the acceleration due to gravity acting on the headform;

$\vec{h}$ is the drop height;

and $\vec{v}$ is instantaneous velocity of the headform. (Hamill & Knutsen, 1995)

Substituting for height:

$$\overrightarrow{v_1} = \sqrt{19.6 \frac{m}{s^2} \times 0.2m} \tag{18}$$

$$\overrightarrow{v_1} = \sqrt{3.92 \frac{m^2}{s^2}}$$

$$\overrightarrow{v_1} = 1.98 \frac{m}{s}$$

Where $\overrightarrow{v_1}$ is the impact velocity for the 0.2m drop height.

$$\overrightarrow{v_2} = \sqrt{19.6\frac{m}{s^2} \times 0.4m} \tag{19}$$

$$\overrightarrow{v_2} = \sqrt{7.84\frac{m^2}{s^2}}$$

$$\overrightarrow{v_2} = 2.80\frac{m}{s}$$

Where $\overrightarrow{v_2}$ is the impact velocity for the 0.4m drop height.

Table E1

Headform Impact Energy and Velocity Summary

Impact Measurement	Drop Height (m)	
	0.2	0.4
Energy	9.8J	19.6J
Velocity	$1.98\frac{m}{s}$	$2.80\frac{m}{s}$

Note. Acceleration due to gravity was given a value of $9.8\frac{m}{s^2}$ for all calculations.